Sustainable Energy & Fuels

Vapor-Fed Electrolysis of Water Using Earth-Abundant Catalysts in Nafion or in Bipolar Nafion/Poly(benzimidazolium) Membranes

Journal:	*Sustainable Energy & Fuels*
Manuscript ID	SE-ART-08-2019-000672.R1
Article Type:	Paper
Date Submitted by the Author:	02-Oct-2019
Complete List of Authors:	Giesbrecht, Patrick; Florida Institute of Technology, Chemistry; Dalhousie University, Chemistry Mueller, Astrid; California Institute of Technology, Beckman Institute; University of Rochester, Chemical Engineering Read, Carlos; California Institute of Technology, Division of Chemistry and Chemical Engineering Holdcroft, Steven; Simon Fraser University, Chemistry Lewis, Nathan; California Institute of Technology, Chemistry and Chemical Engineering Freund, Michael; Florida Institute of Technology, Chemistry; Dalhousie University, Chemistry

ARTICLE

Vapor-Fed Electrolysis of Water Using Earth-Abundant Catalysts in Nafion or in Bipolar Nafion/Poly(benzimidazolium) Membranes

Received 00th January 20xx,
Accepted 00th January 20xx

DOI: 10.1039/x0xx00000x

Patrick K. Giesbrecht;[a,b] Astrid M. Müller;[*c,d] Carlos G. Read;[e] Steven Holdcroft;[*f] Nathan S. Lewis;[*e] Michael S. Freund[*a,b]

Vapor-fed electrolysis of water has been performed using membrane-electrode assemblies (MEAs) incorporating earth-abundant catalysts and bipolar membranes (BPMs). Catalyst films containing CoP nanoparticles, carbon black, and Nafion were synthesized, characterized, and integrated into cathodes of MEAs. The CoP-containing MEAs exhibited stable (>16 h) vapor-fed electrolysis of water at room temperature at a current density of 10 mA cm^{-2} with 350 mV of additional overvoltage relative to MEA's formed from Pt/C cathodic electrocatalysts due to slower hydrogen-evolution reaction kinetics under vapor-fed conditions and fewer available triple-phase boundaries in the catalyst film. Additionally, catalyst films containing a [NiFe]-layered double hydroxide ([NiFe]-LDH) as well as a hydroxide ion conductor, hexamethyl-*p*-terphenyl poly(benzimidazolium) (HMT-PMBI), were synthesized, characterized, and integrated into anodes of MEAs. The [NiFe]-LDH-containing MEAs exhibited overvoltages at 10 mA cm^{-2} that were similar to those of IrO_x-containing MEAs for vapor-fed electrolysis of water at room temperature. A BPM was formed by pairing Nafion with HMT-PMBI, resulting in a locally alkaline environment of HMT-PMBI to stabilize the [NiFe]-LDH and a locally acidic environment to stabilize the CoP. BPM-based MEAs were stable (>16 h) for vapor-fed electrolysis of water at room temperature at a current density of 10 mA cm^{-2}, with a change in the pH gradient of 1 unit over 16 h of electrolysis for IrO_x-containing MEAs. The stability of [NiFe]-LDH-based MEAs under vapor-fed conditions was dependent on the catalyst film morphology and resulting BPM interface, with stable operation at 10 mA cm^{-2} achieved for 16 h. All MEAs exhibited a drift in the operating voltage over time associated with dehydration. These results demonstrate that earth-abundant catalysts and BPMs can be incorporated into stable, room-temperature, vapor-fed water-splitting cells operated at 10 mA cm^{-2}.

.

Introduction

Solar-driven photoelectrochemical water splitting is one approach to the carbon-neutral production of hydrogen.[1] In solar-driven water-splitting devices, the energy in sunlight is captured by semiconducting light absorbers (photoelectrodes) and converted to electrical energy that can drive the two water-splitting half-reactions: hydrogen evolution at the cathode, and oxygen evolution at the anode.[2,3] Electrocatalysts integrated with the surface of the electrodes increase the efficiency of the cell by reducing the kinetic overpotentials for the half-reactions, with the resulting catalyst/electrode assemblies embedded in an electrically and ionically conductive membrane to ensure robust separation of the product gases.

Although solar-driven water-splitting devices have been demonstrated in laboratory settings,[4–11] technological viability requires satisfactorily addressing the earth abundance, cost and long-term operational stability of the materials, as well as efficiency limitations arising from a combination of cell-design-related effects, including highly resistive electrical junctions at the photoelectrode-solution and photoelectrode-membrane interfaces,[12] product-bubble formation, mass-transport limitations, and parasitic light absorption by the solution, catalysts, and membrane.[7]

The use of a water-vapor feed has been proposed as a way of simplifying the overall cell design, providing a purified feedstock without metal ions that can poison the electrocatalysts, and mitigating deleterious effects related to H_2 and O_2 bubble formation in the liquid electrolyte,[13] including light scattering and/or a reduction in the effective areas of the electrode/electrolyte contact and ion-exchange membrane. When water-vapor is fed to the electrode, the vapor condenses on the electrode surface, effectively forming a triple-phase boundary (vapor|water-adlayer|electrode; TPB) similar to the

[a.] *Department of Chemistry, Florida Institute of Technology, Melbourne, Florida 32901, United States.*
[b.] *Department of Chemistry, Dalhousie University, 6274 Coburg Road, Halifax, NS B3H 4R2, Canada.*
[c.] *Beckman Institute, California Institute of Technology, 1200 E. California Boulevard, Mail Code 139-74, Pasadena, California 91125, United States.*
[d.] *Department of Chemical Engineering, University of Rochester, Rochester, New York 14627, United States.*
[e.] *Division of Chemistry and Chemical Engineering, California Institute of Technology, Pasadena, California 91125, United States.*
[f.] *Department of Chemistry, Simon Fraser University, Burnaby, BC V5A 1S6, Canada.*
* *Corresponding authors.* astrid.mueller@rochester.edu; holdcrof@sfu.ca; nslewis@caltech.edu; michael.freund@dal.ca
Electronic Supplementary Information (ESI) available: [details of any supplementary information available should be included here]. See DOI: 10.1039/x0xx00000x

TPB observed in fuel cells. The condensed water adlayer is subsequently electrolysed to produce H_2(g) and O_2(g).[14,15]

Mass-transport and efficiency limitations inherent to triple-phase water splitting (TP-WS) have impeded its adoption in grid-powered water electrolyzers, which typically are operated at high current densities (>1 A cm^{-2} at 80-90 °C) to minimize capital expenditures associated with the area-related balance of systems.[16,17] Electrolysis rates in water-splitting cells driven by unconcentrated sunlight, however, are limited by the terrestrial solar photon flux, and thus will operate at much lower current densities (*ca.* 10 mA cm^{-2}), for which mass-transport of water vapor into the cell, even using moderately humid air, is expected to be sufficient to provide the required current density while ensuring sufficient membrane hydration at room temperature.[13,18] TP-WS has been demonstrated at current densities comparable to the solar photon flux limit using both commercial membrane-electrode assemblies (MEAs)[13,19] and photoelectrochemical systems,[20–23] with ~500 mV overvoltage (cell voltage of 1.7 V) required to split water using unconcentrated sunlight, with the systems stable for >20 h of continuous electrolysis.

Many different earth-abundant semiconductors and electrocatalysts have been developed for water splitting, and most of the materials are sensitive to the local chemical environment (pH, electrolyte, solvent), due to both mechanistic and stability considerations.[24,25] For instance, a CoP catalyst of the hydrogen-evolution reaction (HER) provides overpotentials in acid comparable to Pt, and is stable in acid under 1 Sun photon flux conditions,[26] but the overpotential increases with increasing pH and an amorphous CoO_x surface layer is generated under alkaline conditions.[27,28] Similarly, most earth-abundant electrocatalysts for the oxygen-evolution reaction (OER), such as [NiFe]-layered double hydroxide ([NiFe]-LDH), are only stable under alkaline conditions.[29] Only a few efficient OER catalysts are moderately stable in acidic environments, and with few exceptions such as transition metal antimonates and borides,[30,31] these catalysts generally rely on scarce elements such as Ir and/or Ru.[24]

Bipolar membranes (BPMs) are formed by coupling a cation-exchange membrane (CEM) to an anion-exchange membrane (AEM) (Scheme 1b).[32–34] Unlike monopolar systems (Scheme 1a), bipolar membranes can increase the options for combinations of water-splitting materials by allowing the HER to be performed under locally acidic conditions while the OER is performed under locally alkaline conditions. In a BPM under reverse-bias conditions, water dissociation (WD) occurs at the interface between the CEM and AEM, supplying protons to the cathode and hydroxide ions to the anode. BPMs have been utilized in liquid-phase water-electrolysis cells[8,35] and in an electrolytic flow cell for the reduction of gaseous carbon dioxide, where a decrease in the pH gradient between the anode and the cathode results in a commensurate increase in the operating voltage.[36,37] AEMs and BPMs are promising for TP-WS due to their minimal change in ionic conductivity in fully humidified gas streams relative to their conductivity in solution.[38–40] The development of more cost-effective, solution-processable, and stable AEMs likely will increase efforts to incorporate AEMs into TP-WS systems, as well as into other vapor-based electrolytic cells.[41–43]

This is the first report incorporating both bipolar membranes and earth abundant catalysts in a vapor-fed water electrolyzer. Here, we synthesized and incorporated a highly-active acid-stable, earth-abundant HER catalyst, CoP nanoparticles,[26] and a nanoparticulate [NiFe]-LDH powder (chemical formula $[Ni_{0.78}Fe_{0.22}(OH)_2](NO_3^-)_{0.22}\bullet nH_2O$), a highly-active alkaline-stable, earth-abundant OER catalyst,[44] into separate monopolar and bipolar MEAs for room temperature TP-WS under humid-N_2(g) flow, and evaluated their performance relative to Pt/C|IrO_x-based MEAs. The [NiFe]-LDH film incorporated hexamethyl-*p*-terphenyl poly(benzimidazolium) (HMT-PMBI, Scheme 1c), a recently developed solution-processable AEM that has exhibited long-term stability during electrolysis studies both in monopolar and bipolar configurations,[43,45] and was coupled to a Pt/C film incorporating Nafion (Scheme 1c), a CEM, forming a bipolar MEA. Monopolar and bipolar MEAs were stable for >16 h of constant-current electrolysis, with a reversible voltage drift of 3 mV hr^{-1} during the electrolysis run resulting from gradual dehydration of the membrane and catalyst films. For the bipolar MEAs, this voltage increase would correspond to a pH gradient loss of 0.06 pH units hr^{-1} between the catalyst films over that time period.[46] Larger voltage drifts were observed for CoP-based (5-10 mV hr^{-1}) and [NiFe]-LDH (30-200 mV hr^{-1}) during constant-current electrolysis under humid-N_2(g) due to gradual irreversible catalyst film degradation.

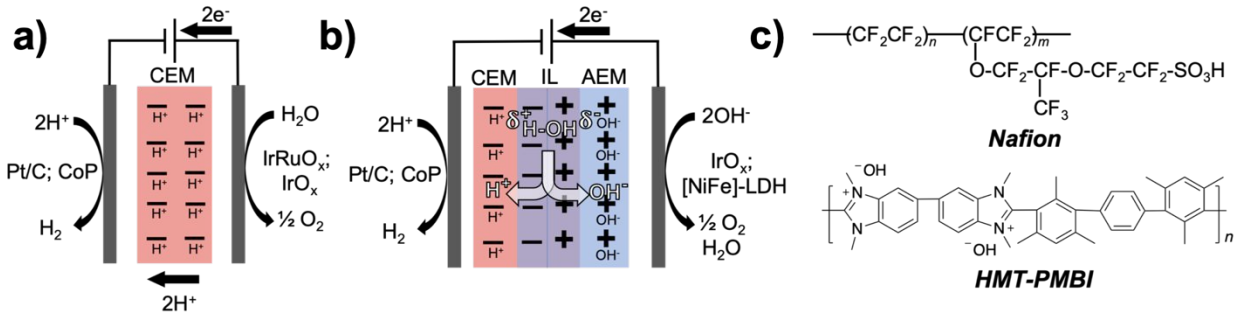

Scheme 1. a) Monopolar membrane configuration for TP-WS, with the catalysts utilized in this work indicated. Water oxidation occurs at the anode, the resulting protons transported through the membrane to the cathode, where hydrogen evolution occurs. b) Bipolar membrane configuration for TP-WS, with the catalysts utilized in this work indicated. Under reverse-bias conditions, hydrogen evolution occurs at the cathode, oxygen evolution occurs at the anode, and water dissociation occurs in the interfacial layer (IL) between the cation exchange membrane (CEM) and the anion exchange membrane (AEM). c) Chemical structures of the CEM (top, Nafion) and AEM (bottom, HMT-PMBI) used to form the MEAs in this work.

Experimental

All chemicals and materials were used as received. MilliQ water was used for all solutions.

Membrane Preparation

Nafion N117 (183 µm thick, Fuel Cell Store) membranes were soaked in water for 1 h at 80 °C, rinsed with water, and stored overnight in 0.50 M H_2SO_4(aq) at room temperature. The membranes were then rinsed with H_2O, placed in water for 1 h, and rinsed again with water before being dried in an oven at 80 °C for 15 min under vacuum.

Hexamethyl-*p*-terphenyl poly(benzimidazolium) solid polymer electrolyte (HMT-PMBI) was synthesized as described previously.[43] HMT-PMBI possessed 89% degree of methylation, which translates to an ion-exchange capacity (IEC) of 2.52 mmol/g in the OH^- form. An HMT-PMBI-based ink was prepared by dissolving HMT-PMBI in the Br-form in methanol under sonication, forming a solution at 5 wt% HMT-PMBI.

Catalyst-ink Preparation

1. Pt

Pt/C (40 wt%, HiSPEC) was dispersed in a water and isopropanol solution (9:1 weight ratio) with Nafion (5wt% aliphatic solution, Sigma) added such that the Pt/C:Nafion weight ratio was 1:0.3. The solution was then ultrasonicated (550 Sonic Dismembrator, Fisher Scientific) for 10 min with a 1 s pulse on/off sequence, with a 5 min break after 5 min. This ink was then painted onto C-paper (200 µm thick, Sigracet 29 BC), or Ti-paper (20 µm fibre diameter, 200 µm thick, Bekaert) on a hotplate at 90 °C until a loading of 3 mg cm^{-2} was obtained. Pt/C films were determined to be 7-10 µm thick using a digital micrometer (Accusize, AC21-1022) prior to MEA formation. For electrochemical experiments using a liquid electrolyte, a Pt-foil (geometric area: 2 cm^2) was used.

2. IrO_x

IrO_2 (Alfa Aesar) was dispersed in methanol with Nafion (5 wt% in aliphatic solution) or HMT-PMBI (5 wt% in methanol) added at a weight ratio of 1:0.1 for IrO_2:Nafion and either 1:0.1 or 1:0.3 for IrO_2:HMT-PMBI. The solution was then ultrasonicated using the sequence described for Pt/C, and the resulting ink was painted onto C-paper on a hotplate until a loading of 3 mg cm^{-2} was obtained. For HMT-PMBI-based inks, the catalyst-loaded C-paper was then soaked in 1.0 M NaOH(aq) overnight, rinsed with H_2O, and dried before use. For electrochemical experiments, the solution containing IrO_2 and Nafion was drop-cast onto a glassy-carbon-disk electrode (3 mm diameter, Basi) at a loading of 2 mg cm^{-2} and baked at 90 °C for 30 min before use. IrO_x catalyst films were determined to be 7-10 µm thick using a digital micrometer (Accusize, AC21-1022) prior to MEA formation.

3. [NiFe]-LDH

[NiFe]-LDH (chemical formula: $[Ni_{0.78}Fe_{0.22}(OH)_2](NO_3^-)_{0.22}\bullet nH_2O$) was synthesized using pulsed-laser ablation in liquids, generating a nanoparticulate powder (<25 nm).[44] The [NiFe]-LDH powder was dispersed in methanol, and HMT-PMBI was added at weight ratios of [NiFe]-LDH:HMT-PMBI of 1:0.1; 1:0.3; and 1:1 ([NiFe]-10, 30, and 100). The ink was ultrasonicated as described above, with the resulting ink then painted onto C-paper on a hotplate at 90 °C until a loading of 0.6 mg cm^{-2} was obtained. For electrochemical experiments, [NiFe]-LDH with 10% HMT-PMBI was drop-cast onto a glassy-carbon-disk electrode until a 0.4 mg cm^{-2} loading was obtained, and before use the sample was baked at 90 °C for 30 min.

4. CoP

The synthesis of spherical, hollow CoP nanoparticles (9-13 nm in size) has been described elsewhere.[26] For loading Ti-paper samples, a CoP suspension in hexanes was air-sprayed onto masked Ti-paper on a hotplate, with the CoP-loaded Ti-paper subsequently annealed for 1 h at 450 °C in a forming gas atmosphere (5% H_2(g), N_2(g) balance), yielding samples with loadings of activated CoP particles of ~2.5 mg cm^{-2} on the Ti-paper. To provide a Nafion overcoat, the loaded CoP samples were soaked in a 1 wt% Nafion solution and baked at 100 °C. The soaking and baking steps were repeated until 5 total iterations had been completed.

Using a similar preparation, an activated form of CoP as a powder was developed, in which the as-made nanoparticles suspended in hexanes were dried under vacuum and subsequently annealed for 1 h at 450 °C in a forming gas atmosphere (5% H_2(g), N_2(g) balance). The CoP powder was then dispersed in a water-isopropanol mixture (weight ratio of 1:0.1) with Nafion added at 30 wt% relative to CoP (5 wt% in aliphatic solution) and C black added in at a 1:1 ratio to CoP. The Nafion and C black were added into the film to increase the electrical conductivity of the film and promote the adhesion of the film to the electrode surface. The mixture was ultrasonicated following the procedure as described above and was painted onto C-paper on a hotplate at 90 °C until a loading of 2 mg cm^{-2} was obtained. To minimize particle loss based on preliminary TP-WS results (see Figure S3), the sample was then iteratively dip-coated in 1 wt% Nafion solution and baked at 100 °C, for a total of five iterations. The preparation of the CoP films used for three-electrode studies in liquid electrolyte was the same as for films used for TP-WS.

MEA Formation

MEAs were prepared by heat-pressing (YLJ-HP60-LD, MTI Corporation) the HER- and OER-catalyst-loaded C-paper or Ti-paper to a Nafion membrane (N117, 183 µm thick, Fuel Cell Store) between PTFE gaskets (100 µm thick, Fuel Cell Store) at 130 °C and 500 psi for 120 s. None of the catalysts were observed to decompose during the MEA preparation steps performed in this work. Current densities were determined using the geometric surface area of the catalyst layer (3 cm^2).

Electrochemical Methods

A CHI 660C potentiostat, a graphite rod counter electrode, and a Ag/AgCl aqueous quasi-reference electrode were used for three-electrode experiments using the working electrodes described above. Polarization studies were performed at scan rates of 25-100 mV s^{-1}, in either acidic (0.50 M H_2SO_4(aq)) or alkaline (1.0 M KOH(aq)) electrolytes. All measured potentials were converted to, and reported versus, RHE. *iR*-corrected data was determined by subtracting the voltage contribution associated with solution resistance at that current from the

measured potential and was used for Tafel analysis. In circumstances where there was a significant background current associated with double-layer charging, this was also subtracted from the HER/OER current response before performing Tafel analysis.

Electrolytic Cell Characterization

TP-WS was performed in a two-electrode configuration using a gas-flow cell with two graphite end plates each with serpentine flow channels (Fuel Cell Store) and a Solartron 1287 potentiostat with a 1255B frequency-response analyser. The cell setup is depicted in Figure 1. Ultra-high purity (UHP) N_2(g) was bubbled through H_2O(l) to generate a humid-N_2(g) flow prior to entry into the cell, and passed through the cathode and anode compartments of the cell at a rate of 0.2 L min^{-1} to ensure the rate of mass-transport of water to the MEA was sufficient to support the current densities used in the experiments.[13] Due to the necessity of high relative humidity (RH) for optimal vapor-phase conductivity of the AEM, all studies were conducted at >95%RH to allow for accurate comparison and to determine the feasibility of AEM incorporation in TP-WS. Steady-state polarization data were obtained by taking 50 mV steps from the open-circuit voltage to 3 V versus the open-circuit voltage, with the current measured for 150 s for each data point. EIS studies were performed at voltages that produced a current density of 10 mA cm^{-2}, using an amplitude voltage of 10 mV and a frequency range of 0.1-100000 Hz. Electrical noise prevented EIS studies from being performed at lower frequencies. *iR*-corrected data was determined by subtracting the measured voltage by the contribution associated with the series resistance, obtained by EIS at an operating voltage to supply 10 mA cm^{-2}, and was used for Tafel analysis. In circumstances where there was a contribution due to background current associated with double-layer charging, this was also subtracted from the current response associated with TP-WS before performing Tafel analysis. Constant-current studies were conducted at a current density of 10 mA cm^{-2} over a period of 16 h. Rehydration of MEAs was achieved by exposing the MEA to humid-N_2(g) flow under open-circuit conditions until a stable open-circuit voltage was obtained. To validate all electrolytic processes conducted in this work, a commercially available Pt/C|$IrRuO_x$ catalyst-coated membrane (3.0 mg cm^{-2} catalyst loadings, 127 µm thick Nafion membrane, FuelCellStore) was used with C-paper placed on both the anode and cathode side to minimize the electrical resistance of the MEA.

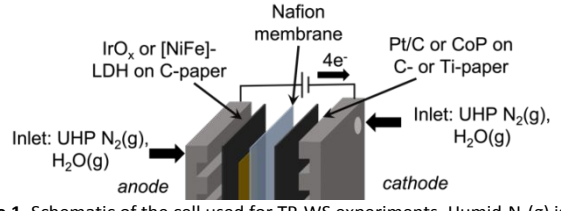

Figure 1. Schematic of the cell used for TP-WS experiments. Humid-N_2(g) is fed to the anode and cathode compartments, allowing TP-WS to be performed.

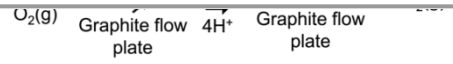

Materials Characterization

Anode and cathode films were characterized before MEA incorporation *via* Scanning Electron Microscopy (SEM) using a JEOL JSM-6380LV SEM instrument using an acceleration voltage of 10 kV. All films were conductive and were characterized uncoated.

Results

Catalyst films

The electrocatalytic performance of CoP nanoparticles activated directly on the electrode surface (CoP-Ti) was compared in a three-electrode configuration in contact with 0.50 M H_2SO_4(aq) (Figure 2a), with a graphite rod counter electrode, to a nanoparticulate CoP powder that was activated in the same manner and spray-coated onto C-paper (see Experimental) for HER. The performance of a Pt foil for the HER in contact with 0.50 M H_2SO_4(aq) in a three-electrode configuration is also shown. Both the CoP film on Ti-paper (CoP-Ti) and the CoP film on C-paper (CoP-C) were dip-coated in Nafion prior to operation to minimize CoP particle loss. At a cathodic current density of 10 mA cm^{-2}, the CoP films required an overpotential ($\eta_{-10\ mA\ cm^{-2}}$) of ~ -65 mV to drive the HER, whereas the Pt foil required $\eta_{-10\ mA\ cm^{-2}}$ = -45 mV, tabulated in Table S1, consistent with previous results.[26] The current generated at ~ 0 V versus the reversible hydrogen electrode (RHE) is the result of non-Faradaic processes and double-layer charging of the electrodes (geometric area of 1-5 cm^2), as opposed to the operation of HER.

The current density associated with an electrocatalyst to perform a catalytic reaction in solution can be related to the

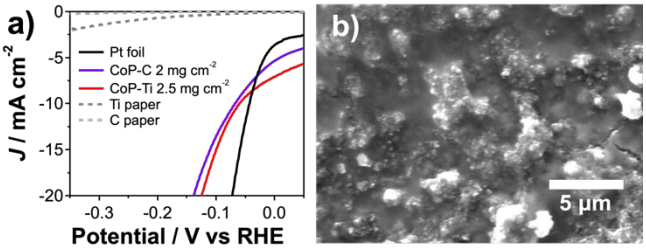

overpotential associated with the catalytic event by the Butler-Volmer equation:[47]

$$J = J_0 [\exp(-\alpha n F\eta/RT) - \exp((1-\alpha)nF\eta/RT)] \quad (1)$$

$$J = J_0 \exp(-\alpha n F\eta/RT) \quad (2)$$

$$J = J_0 \exp((1-\alpha)nF\eta/RT) \quad (3)$$

Where J is the current density, J_0 the exchange current density, n the number of electrons transferred, α the charge transfer coefficient ($n\alpha$ the effective charge transfer coefficient), F is Faraday's constant, η the overpotential, R the gas constant and T the temperature of the system. At sufficiently large overpotentials for the catalytic event, where the forward reaction rate is sufficiently larger than the reverse reaction rate, Equation 1 reduces to Equation 2 for a reduction process, and Equation 1 reduces to Equation 3 for an oxidation

process. This allows values of nα (or n(1-α)) and J_0 to be determined empirically using the Tafel relation,

$$\eta = (2.303RT/ n\alpha F)\log(J_0) - (2.303RT/ n\alpha F)\log(J) \quad (4)$$
$$\eta = (2.303RT/ n(1-\alpha)F)\log(J_0) - (2.303RT/ n(1-\alpha)F)\log(J) \quad (5)$$
$$\eta = a + b\log(J) \quad (6)$$

where *a* is the intercept of the extrapolated Tafel plot based on experimental data, and *b* the Tafel slope, reported in mV dec^{-1}. The Tafel slope provides insight towards the rate-determining step of the process, corresponding to a value of nα (n(1-α)), while J_0 is related to the intrinsic catalytic activity of the catalyst.

Under acidic conditions, HER can be described as a three-step hydronium ion reduction:[47]

$M + H_3O^+ + e^- \rightarrow M\text{-}H + H_2O$ (Volmer step)
$M\text{-}H + H_3O^+ + e^- \rightarrow H_2 + H_2O + M$ (Heyrovsky step)
$2M\text{-}H \rightarrow H_2 + 2M$ (Tafel step)

where M denotes an empty surface site on the catalyst. The Tafel slope changes based on the rate determining step, where these processes correspond to 'characteristic' Tafel slopes of 120, 40, and 30 mV dec^{-1} (nα= 0.5, 1.5, 2) for HER operation, respectively, assuming a surface-coverage independent process.

For OER, the mechanism is more complicated, as four electrons are involved in the mechanism, with the process surface-dependent, resulting in numerous pathways proposed.[47–49] It has been observed that IrO_x, undergoes the 'Krasil'shchikov path' in acidic solution,[49]

Krasil'shchikov path:

$M + H_2O \rightarrow MOH + H^+ + e^-$ (step 1)
$MOH \rightarrow MO^- + H^+$ (step 2)
$MO^- \rightarrow MO + e^-$ (step 3)
$MO \rightarrow M + ½\ O_2$ (step 4)

For this pathway, assuming a potential independent Tafel slope, Tafel slopes of 120, 59, 40, and 30 mV dec^{-1} are expected for steps 1 through 4 (n(1-α)= 0.5, 1, 1.5, 2). The exact mechanism under alkaline conditions is still unclear given the large dependence on surface sites present during electrolysis,[47,50] and as such we report the Tafel slopes and corresponding values of n(1-α) determined in this work.

To determine if the kinetics of HER in solution by CoP was affected by the addition of a Nafion layer, Tafel plots of iR-corrected overpotentials were evaluated assuming Butler-Volmer kinetics (Equations 4&6; Figure S1a). A Tafel slope of 29 mV dec^{-1}, corresponding to a value of nα of 2, was obtained for Pt foil, consistent with previous results and a Tafel rate-limiting step.[47] CoP-Ti exhibited a Tafel slope of 49 mV dec^{-1} (nα = 1.2), consistent with previous reports,[26] while CoP-C exhibited a potential dependent Tafel slope, initially 132 mV dec^{-1} (-0.15 V<η<-0.05 V vs RHE), corresponding to a value of nα of 0.45, suggesting a Volmer rate-limiting step,[47] and decreased to 44 mV dec^{-1} at higher (<-0.05 V vs RHE) η (nα = 1.3).[26] J_0 for Pt foil was determined to be 0.9 mA cm^{-2}, while the CoP-Ti sample was found to have a J_0 of 0.1 mA cm^{-2}, consistent with previous reports.[26] The potential dependent Tafel slope for CoP-C prevented accurate determination of J_0 for HER in acidic solution. These results suggest that while $\eta_{-10\ mA\ cm^{-2}}$ was not affected by the addition of a Nafion layer or incorporation of CoP catalysts into ink preparations, the rate-limiting step (Tafel slope) for CoP-C-paper-based films was altered at low η (>-0.05 V vs RHE) in a liquid acidic electrolyte. The use of a Nafion overcoat was found to not affect the activity of CoP-Ti-based films towards HER in acidic solution. Scanning-electron micrographs (SEM) of a CoP-C sample (Figure 2b), show that the CoP particles are uniformly coated or embedded in the Nafion polymer matrix after the dip-coating procedure. In contrast, Pt/C films on C-paper exhibit a porous structure (Figure S2a).

The electrocatalytic performance of [NiFe]-LDH was compared to IrO_x, both deposited on glassy-carbon-disk electrodes, for OER in a three-electrode configuration in contact with 1.0 M KOH(aq), with a graphite counter electrode (Figure 3a). The value of $\eta_{10\ mA\ cm^{-2}}$ was found to be 300 mV or 286 mV for IrO_x and [NiFe]-LDH (Table S1) in this work, consistent with previous reports.[22,44] A shoulder is observed in the [NiFe]-LDH anodic sweep at low η_{OER} , resulting from the oxidation of Ni^{2+} to Ni^{3+} in the catalyst film.[51] Analysis of the Tafel plot (Equations 5&6; Figure S1b) for the IrO_x film provided a Tafel slope of 55 mV dec^{-1} at large overpotentials (η >270 mV), corresponding to a value of n(1-α) of 1, consistent with previous reports.[47,52] The [NiFe]-LDH film also exhibited a potential-dependent Tafel slope, 25 mV dec^{-1} at low (η <270 mV; n(1-α) of 2.5), smaller

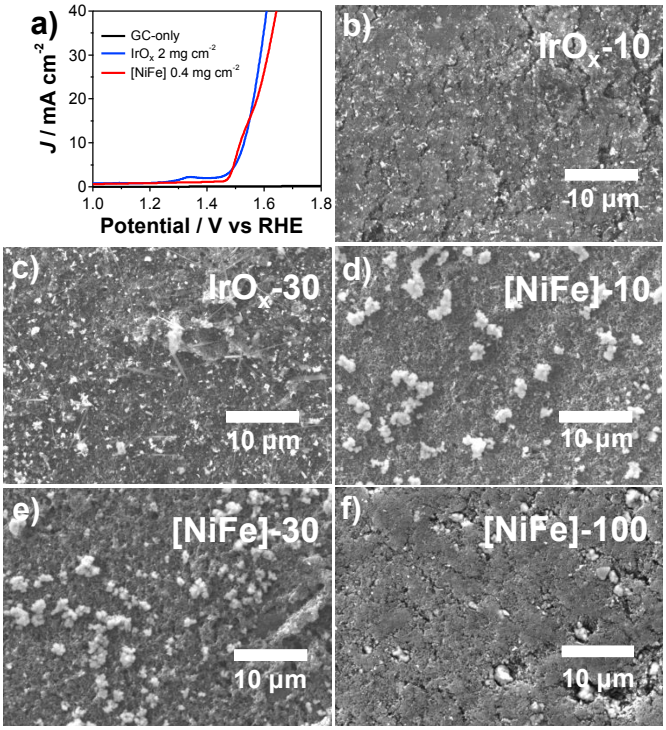

Figure 3. a) Uncorrected polarization data for IrO_x (blue) and [NiFe]-LDH (red) on glassy-carbon-disk electrodes in a three-electrode configuration in contact with 1.0 M KOH(aq) at catalyst loadings of 2 mg cm^{-2} and 0.4 mg cm^{-2}, respectively. The scan rate was 50 mV s^{-1}. b-c) Scanning-electron micrographs of IrO_x films with 10 or 30 wt% HMT-PMBI in the film relative to IrO_2. d-f) Scanning-electron micrographs of [NiFe]-LDH with 10, 30, or 100 wt% HMT-PMBI in the films relative to [NiFe]-LDH.

than the 30-40 mV dec^{-1} observed in previous reports,[53] and 63 mV dec^{-1} at higher η. Both Tafel slopes reported for [NiFe]-LDH OER operation are convoluted with the Ni-oxidation process observed at the potentials measured, resulting in this discrepancy. J_0 was determined to be 5x10^{-5} mA cm^{-2} for IrO_x, comparable to previous reports,[52] while the [NiFe]-LDH film was found to have a J_0 of 2x10^{-11} mA cm^{-2}, based on extrapolation of the Tafel plot. Since the OER is highly irreversible, resulting in a large difference between the currents measured and the determined J_0, the exchange current densities determined here do not offer an accurate comparison of the intrinsic catalyst activity towards OER.[54] Incorporation of HMT-PMBI into the OER catalyst film was found to not affect the kinetics of OER in alkaline solution.

[NiFe]-LDH and IrO_x catalyst films prepared with varied HMT-PMBI content exhibit a porous structure on C-paper (Figure 3), similar to the morphology of an IrO_x-Nafion film (Figure S2b). Increasing the HMT-PMBI content in [NiFe]-LDH films led to uniform embedding of [NiFe]-LDH particles in a porous polymer matrix and reduced the amount of [NiFe]-LDH observed on the catalyst film surface.

Triple-Phase Water Splitting

1.CoP|IrO_x Nafion MEAs

The performance of the earth-abundant catalysts to effect TP-WS was determined by fabricating MEAs and operating the system in a two-electrode configuration under humid-N_2(g) flow at room temperature using a flow cell with serpentine gas channels (see Experimental). This configuration allowed measurement of the required operating voltage, V, and consequently measurement of the overvoltage, ΔV, relative to the 1.18 V thermodynamic voltage, based on the change in free energy involved with producing H_2(g) and ½ O_2(g) from H_2O(g) under standard-state conditions at room temperature.[13] An expression for the total overvoltage at an applied current density is shown in Equation 7, where ΔV is composed of the product of the current and the electrical/ionic resistances of the membrane/catalyst films/flow cell (ΔV_{iR}), activation overvoltages associated with the kinetics of TP-WS by the HER and OER catalysts (ΔV_{act}), and a mass-transport related overvoltage (ΔV_{mxt}).

$$\Delta V_{total} = \Delta V_{iR} + \Delta V_{act} + \Delta V_{mxt} \qquad (7)$$

At nominally comparable catalyst loadings, the custom Pt/C|IrO_x MEA used in this work exhibited a 150±10 mV larger operating voltage to pass 10 mA cm^{-2}, $V_{10\ mA\ cm^{-2}}$, than a commercially available Pt/C|$IrRuO_x$ MEA (Figure S3a). Analysis of the steady-state polarization data indicates that mass-transport-related processes result in a minimal overvoltage (<5 mV) for both MEAs at 10 mA cm^{-2}, confirming that the majority of the overvoltage observed is the result of catalyst activation in this regime for TP-WS (see SI for calculations). Under constant-current electrolysis at 10 mA cm^{-2}, $V_{10\ mA\ cm^{-2}}$ of the Pt/C|IrO_x MEA voltage increased 50 mV after 16 h, with the initial operating voltage obtained after rehydration of the MEA at open-circuit for 15 minutes (Figure S8a). No drift in $V_{10\ mA\ cm^{-2}}$ was observed for the Pt/C|$IrRuO_x$ MEA after 16 h. This behaviour was reproducible for multiple Pt/C|IrO_x MEAs prepared in the same manner (Figure S7, Table S3), suggesting a drift associated with MEA dehydration rather than MEA flooding. To ensure reproducibility of the cell, a steady-state polarization study of a Pt|IrO_x MEA as well as the Pt|$IrRuO_x$ MEA was taken, the cell disassembled, reassembled with the same MEA, rehydrated, and a second steady-state polarization study conducted, with no change observed in the data obtained. These results suggest this increased dependence on water vapor availability and difference in TP-WS performance observed for the Pt/C|IrO_x MEA relative to the Pt/C|$IrRuO_x$ MEA is due to differences in preparation steps taken, HER/OER catalyst film compositions/syntheses, and resulting catalyst film structures/catalyst-membrane interfaces.[55]

The CoP nanoparticulate powder produced in this work offers the ability to form composite catalyst films through the addition of C-black and Nafion into the catalyst film to potentially improve the TP-WS capabilities of the MEA (optimizations shown in Figure S4), as well as afford a more direct comparison of the TP-WS capabilities of CoP relative to Pt/C. Initial constant-current electrolyses conducted at 10 mA cm^{-2} of CoP-Ti and CoP-C-containing MEAs without a Nafion overcoat exhibited a large increase in the operating voltage over time due to gradual CoP particle loss from the catalyst film (Figure S4a). The addition of a Nafion overcoat minimized CoP particle loss but limited the porosity of the resulting catalyst film necessary for TP-WS (Figure 2b).

Comparison of the TP-WS characteristics of the resulting CoP|IrO_x MEAs with the TP-WS characteristics of a Pt/C|IrO_x MEA is shown in Figure 4a. The MEAs with CoP on either C-paper or Ti-paper required an additional 360-370 mV in $V_{10\ mA\ cm^{-2}}$ relative to the Pt/C|IrO_x MEA (Table 1). For CoP-based MEAs, there was no observable difference in $\Delta V_{10\ mA\ cm^{-2}}$ between CoP-C and CoP-Ti-based MEAs during steady-state polarization studies. Both CoP-C and CoP-Ti MEAs with a Nafion overcoat exhibited a drift of 100-190 mV during constant-current electrolysis at 10 mA cm^{-2} that was, in part, the result of gradual MEA dehydration (Figure S8).

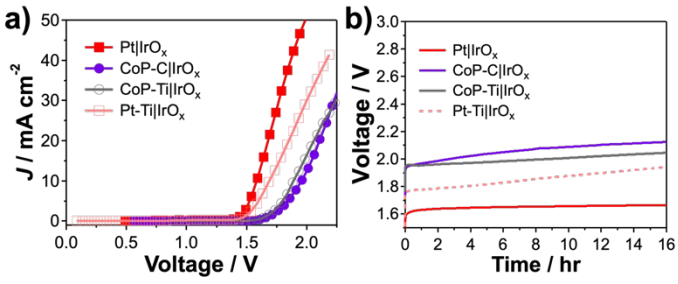

Figure 4. a) Steady-state polarization data for TP-WS under humid-N_2(g) flow at room temperature in a two-electrode configuration for Nafion MEAs using Pt/C on C-paper (3 mg cm^{-2}, red solid squares), Pt/C on Ti-paper (3 mg cm^{-2}, pink open squares), CoP on C-paper (2 mg cm^{-2}, purple solid circles), or CoP on Ti-paper (2.5 mg cm^{-2}, grey open circles) as the cathode. b) Constant-current electrolysis (10 mA cm^{-2}) data for TP-WS under humid-N_2(g) flow at room temperature in a two-electrode configuration Pt/C and CoP samples on C-paper or Ti-paper as the cathode. All MEAs utilized IrO_x (3 mg cm^{-2}) with Nafion binder on C-paper as the anode.

To confirm this influence of the MEA preparation used for Ti-paper CoP samples on $\Delta V_{10\ mA\ cm^{-2}}$ for TP-WS, the TP-WS characteristics of MEAs made using Pt/C on C-paper were compared to those for MEAs made using Pt/C on Ti-paper with a Nafion overcoat. The value of $\Delta V_{10\ mA\ cm^{-2}}$ was 100 mV larger for the MEA with Pt/C on Ti-paper than for the MEA with Pt/C on C-paper based on steady-state polarization data (Table 1), and was found to drift 190 mV during constant-current electrolysis at 10 mA cm^{-2} due to MEA dehydration and gradual MEA degradation (Table S3). The Pt/C-Ti MEA exhibited a large (*ca.* 9 Ω cm^2) series resistance comparable to that observed for the CoP-Ti MEA (Table S2).

Electrochemical impedance spectroscopy (EIS) measured *in situ* during TP-WS at the operating voltage $V_{10\ mA\ cm^{-2}}$ was used to determine (i) the series resistance due to the ionic and electronic resistances in the MEAs (Z' intercept of Nyquist plot at high frequency), corresponding to ΔV_{iR}, (ii) the polarization resistance associated with the kinetics of TP-WS (width of Nyquist spectra plot) of the MEAs, corresponding to a polarization overvoltage $\Delta V_{polarization}$, and (iii) determination of the contribution and corresponding resistance of the individual catalyst films towards TP-WS operation. Figure 5 shows Nyquist plots of the EIS data for representative MEAs studied in this work at the operating voltage $V_{10\ mA\ cm^{-2}}$ required to drive TP-WS in a two-electrode configuration under humid-N_2(g) flow at room temperature, with the corresponding Bode plots provided in the SI (Figure S9). The obtained resistance values were then converted into overvoltages, ΔV_{iR} and $\Delta V_{polarization}$, based on the current density passed (10 mA cm^{-2}), allowing their contribution to $\Delta V_{10\ mA\ cm^{-2}}$ to be determined and tabulated in Table S2.

Pt/C-containing and CoP-containing Nafion-based MEAs exhibited a small high frequency depressed semicircle and a large low frequency depressed semicircle. These spectra were fit to the circuit shown in Figure 5b, a series resistance R_s corresponding to ionic/electrical resistances of the cell/membrane, a resistor (R_{cath}) in parallel with a constant-phase element (CPE, Q_{cath}) corresponding to HER operation by the cathode, and a resistor (R_{an}) in parallel with a CPE (Q_{an}) corresponding to OER operation by the anode, with the values obtained and fits shown in the SI (Figure S10, Table S4). CPE elements rather than capacitors were used to account for deviations in the capacitance due to catalyst film surface roughness, non-homogeneous interfaces, and catalyst polycrystallinity in the MEAs.[56]

For Pt|IrO_x MEAs, the small high frequency depressed semicircle corresponds to HER operation at the Pt-catalyst film, while the large low frequency depressed semicircle corresponds to OER operation at the IrO_x-catalyst film. This result agrees with the EIS spectra of similar MEAs in both liquid water and electrolyte, where the impedance is found to be predominantly from the anode despite the same catalyst loadings due to differences in catalytic ability (i.e., J_0).[57] For CoP-based MEAs, the small high frequency depressed semicircle was found to instead correspond to OER operation at the anode film, while the large depressed semicircle at lower frequencies corresponds to HER operation at the CoP-catalyst film. The majority of the impedance results from the CoP-catalyst film despite comparable catalyst loadings in the IrO_x-anode in CoP-based MEAs, suggesting slower kinetics performing HER in TP-WS relative to OER operation by IrO_x in TP-WS, the opposite of that observed in a three-electrode configuration in acidic electrolyte.[26,52] A large series resistance is observed for the CoP-Ti MEA, consistent with the Pt-Ti MEA results, associated with the use of Ti-paper and a Nafion overcoat, whereas CoP-C MEAs exhibit a series resistance comparable to Pt/C-C-paper systems. The impedance of a CoP-C MEA after constant-current electrolysis and after rehydration of the MEA shows a 20 mV increase in $\Delta V_{polarization}$, with only a small, 2 mV, increase in the series voltage, suggesting gradual CoP film deactivation or degradation during TP-WS. No impedance resulting from mass-transport was observed in any of the monopolar MEAs at the frequencies investigated (>0.1 Hz, see Experimental), suggesting again that mass-transport has a minimal impact on the overvoltage under the conditions utilized for TP-WS.

The EIS data were also used to generate *iR*-corrected TP-WS polarization data for representative MEAs in this study (Figure 7a) by removing the contribution to the polarization data by ΔV_{iR}. This allows a direct comparison between ΔV_{act} of different

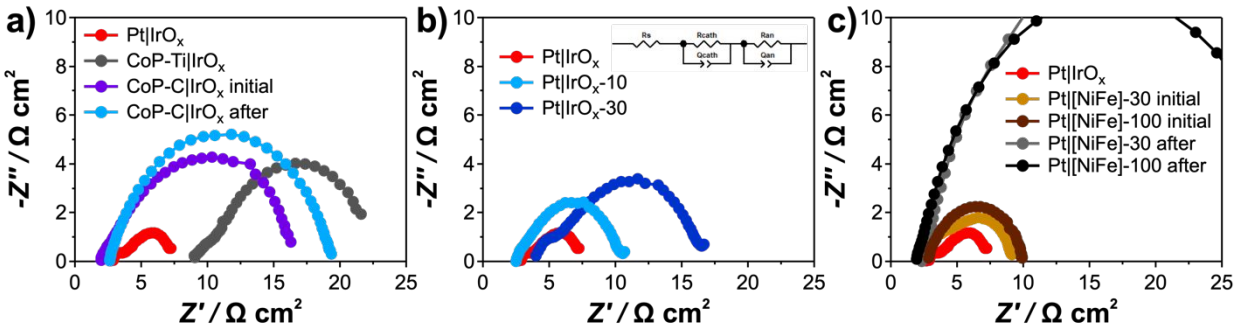

Figure 5. Nyquist plots for MEAs performing TP-WS at $V_{10\ mA\ cm^{-2}}$ in a two-electrode configuration under humid-N_2(g) flow at room temperature with a) CoP-Ti (2.5 mg cm^{-2}, grey circles) and CoP-C cathodes before (2 mg cm^{-2}, purple circles) and after (light blue circles) constant-current electrolysis at 10 mA cm^{-2} under humid-N_2(g) flow at room temperature. The anode was IrO_x (3 mg cm^{-2}) on C-paper. Nyquist plots for MEAs performing TP-WS at $V_{10\ mA\ cm^{-2}}$ in a two-electrode configuration under humid-N_2(g) flow at room temperature with b) IrO_x with 10 wt% HMT-PMBI (3 mg cm^{-2}, light blue circles) and 30 wt% HMT-PMBI (3 mg cm^{-2}, dark blue circles), or c) [NiFe]-LDH with 30 wt% HMT-PMBI (0.6 mg cm^{-2}, gold circles) and 100 wt% HMT-PMBI (0.6 mg cm^{-2}, brown circles) anodes before and after (grey and black circles, respectively) constant-current electrolysis at 10 mA cm^{-2} under humid-N_2(g) flow at room temperature. The cathode was Pt/C (3 mg cm^{-2}) on C-paper. A Nyquist plot for Nafion-based Pt/C|IrO_x MEA (red circles) performing TP-WS at $V_{10\ mA\ cm^{-2}}$ under humid-N_2(g) flow at room temperature is shown for comparison. Inset of b) is the equivalent circuit used to model the obtained EIS spectra for MEAs in this work.

MEAs in this work to perform TP-WS under humid-N_2(g) flow at room temperature, with the values tabulated in Table S2 for a current density of 10 mA cm^{-2}. Tafel plots were also generated, where the Tafel slope corresponds to the kinetics of the rate-limiting catalyst film in the MEA (Figure 7c). The rate-limiting catalyst film was determined based on the catalyst film contribution to the EIS spectra in Figure 5 (Figure S10, Table S4) under TP-WS conditions. Due to the chemical irreversibility of TP-WS under our experimental conditions (humid-N_2(g) flow), as well as the irreversibility of the OER process (slow electron transfer kinetics), only the Tafel slopes can be accurately determined for TP-WS, and are reported here.[54,58] MEAs containing Pt/C cathodes were found to exhibit similar ΔV_{act} at all current densities measured when deposited on C-paper or Ti-paper, indicating that the use of Ti-paper and the Nafion overlayer only resulted in an increase in the series resistance for Pt-based MEAs. Both Pt-based MEAs exhibit a linear region in the Tafel plot within the current regime of interest (1-20 mA cm^{-2}), with the Tafel slope increasing at higher current densities due to mass-transport limitations.

The Tafel slope in the linear region was determined to be 121±1 and 127 mV dec^{-1} for Pt-C and Pt-Ti-based MEAs, tabulated in Table 1, with the error reported resulting from multiple MEAs. The main contribution to the Tafel slope is from the IrO_x anode based on the EIS analysis, and as such, represents the kinetics at the Nafion-based anode. The Tafel slope (~120 mV dec^{-1}; n(1-α) = 0.5) is larger than the values expected from acidic solution studies (55 mV dec^{-1}),[52] and suggests, based on the Krasil'shchikov path under acidic conditions, that the initial surface adsorption process is the rate determining step (step 1: $M + H_2O \rightarrow MOH + H^+ + e^-$) under TP-WS operation.[47,48] While there have been no reported Tafel slopes for TP-WS Nafion-based OER, this increase in the Tafel slope to 100-120 mV dec^{-1} under TP-WS conditions relative to solution-based conditions has been observed for HER and hydrogen oxidation reaction catalysts such as Pt/C and Ir/C in Nafion-based fuel cell setups.[58] An increase in the Tafel slope has also been associated with ionic transport losses in the catalyst film in polymer electrolyte-based fuel cells, where the catalyst films in the MEA behave similar to flooded diffusion electrodes, resulting in a double Tafel slope that is dependent on the diffusion of reactants into the MEA.[59,60]

CoP-based MEAs were found to have a ΔV_{act} that was dependent on the preparation procedure, where CoP-Ti MEA exhibits a lower ΔV_{act} for all current densities studied (0.60 V @ 10 mA cm^{-2}) relative to the CoP-C MEA (0.75 V @ 10 mA cm^{-2}). Since the main contributor to the impedance of CoP-based MEAs was determined to be the CoP cathode rather than IrO_x, ΔV_{act} and the resulting Tafel plot corresponds to the kinetics at the CoP cathode. A linear region from 0.5-20 mA cm^{-2} in the Tafel plot of CoP-Ti MEAs is observed, corresponding to a slope of 152±16 mV dec^{-1} (nα = 0.39). The CoP-C MEA was found to have a voltage-dependent Tafel slope, where a minimum value of 157 mV dec^{-1} is observed at low currents (0.1-1 mA cm^{-2}). The Tafel slope for both CoP-based MEAs under TP-WS operation were larger than the characteristic Tafel slopes associated with HER operation (30, 40, and 120 mV dec^{-1}),[47] potentially due to the application of a Nafion overcoat (Figure 2b).

Table 1 Operating voltage for TP-WS at 10 mA cm^{-2}, with corresponding $\Delta V_{10\ mA\ cm^{-2}}$ and Tafel slope for TP-WS of water vapor at room temperature.

MEA	$V_{10\ mA\ cm^{-2}}$ (V)[a]	$\Delta V_{10\ mA\ cm^{-2}}$ (V)[b]	Tafel Slope (mV dec^{-1})[c]
Pt|IrO_x[d]	1.59±0.01	0.41±0.01	121±1
Pt|IrO_x-10	1.74±0.02	0.56±0.02	226±11
Pt|IrO_x-30	1.84±0.09	0.66±0.09	220±10
CoP-Ti|IrO_x	1.95±0.05	0.77±0.05	152±16
CoP-C|IrO_x	1.96	0.78	157
Pt-Ti|IrO_x	1.70	0.52	127
Pt|[NiFe]-10	1.73±0.01	0.55±0.01	106±6
Pt|[NiFe]-30	1.74±0.03	0.56±0.03	108±14
Pt|[NiFe]-100	1.70±0.01	0.52±0.01	97±10

[a]Operating voltage at 10 mA cm^{-2} as determined from steady-state polarization data. [b]Overvoltage associated with TP-WS at 10 mA cm^{-2} of water vapor (E^0 = 1.18 V). [c]Tafel slope determined from *iR*-corrected polarization data. Values reported are replicate sample averages (n=2), with the standard deviation shown. [d]Values reported for replicate samples (n=3).

2. Bipolar MEAs

Introduction of HMT-PMBI into the anode film, as opposed to Nafion as the ionomer, results in the formation of an asymmetric bipolar membrane that can undergo TP-WS while sustaining a pH gradient between the anode (alkaline) and cathode (acidic). This results in an interfacial region depleted of mobile ions at the Nafion|HMT-PMBI interface that impedes charge transport until WD is initiated under reverse bias conditions.[33] The interfacial layer at the Nafion|HMT-PMBI interface is reported to be 9 nm thick, and can grow over time if the supply of water to the interface is insufficient to match the current density applied, resulting in a reversible increase in the series resistance of the MEA.[45]

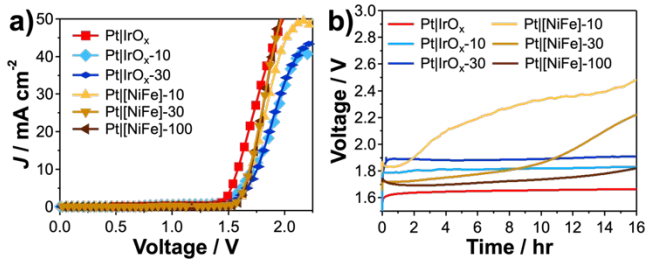

Figure 6. a) Steady-state polarization data and b) constant-current electrolysis (10 mA cm^{-2}) data for TP-WS in a two-electrode configuration under humid-N_2(g) flow at room temperature by MEAs using IrO_x with a Nafion binder (red squares), IrO_x with 10 wt% HMT-PMBI (light blue diamonds), IrO_x with 30 wt% HMT-PMBI (dark blue diamonds), [NiFe]-LDH with 10 wt% HMT-PMBI (yellow triangles), [NiFe]-LDH with 30 wt% HMT-PMBI (gold triangles), or [NiFe]-LDH with 100 wt% HMT-PMBI (brown triangles) on C-paper as the anode. IrO_x loading of 3 mg cm^{-2}, [NiFe]-LDH loading of 0.6 mg cm^{-2}. Pt/C on C-paper (3 mg cm^{-2}) was used as the cathode for all MEAs. Wt% of HMT-PMBI is relative to the mass of anode catalyst used.

The stability of HMT-PMBI during TP-WS electrolysis experiments in a two-electrode configuration under humid-N_2(g) flow was determined by incorporating HMT-PMBI, instead of Nafion, into IrO_x anodes, at 10 wt% or 30 wt% of IrO_x (Figure 6). The HMT-PMBI-containing MEAs (IrO_x-10, IrO_x-30) exhibited an additional 150±20 mV or 250±90 mV, respectively, in $V_{10\ mA\ cm^{-2}}$, relative to the Nafion-only IrO_x MEAs (Table 1). A drift in this operating voltage was observed during constant-current electrolysis at 10 mA cm^{-2} under humid-N_2(g) flow (30-50 mV, Table S3) and was found to return to initial values upon application of the rehydration procedure (Figure S8), indicating that either the MEA was dehydrated or that co-ion current that results in double-layer charging in the catalyst films was the predominant current. Calculations based on the thickness and area of the membrane and catalyst films, and known ion-exchange concentrations (1.5 M for both Nafion and HMT-PMBI)[43] show that if co-ions were the predominant species in the film and co-ion current was the only pathway to pass charge (WD was not occurring at the interface), and since the MEA is not in contact with an electrolyte solution, this process would last *ca.* 300 s when applying a current density of 10 mA cm^{-2} (see SI for calculations) before a significant increase in the operating voltage is observed. The drift observed is therefore likely the result of gradual dehydration of the MEA during operation, where the predominant current generation at the interface is through WD.

Nyquist plots of BPM IrO_x-based MEAs at the operating voltage $V_{10\ mA\ cm^{-2}}$ required to drive TP-WS in a two-electrode configuration under humid-N_2(g) flow at room temperature are shown in Figure 5b, where similar to the Nafion-only system, two depressed semicircles are observed corresponding to the cathode and anode kinetics. It is expected that an additional contribution associated with WD is contained within the impedance spectra, but is convoluted with the anode OER kinetics.[61] A 20 mV or 80 mV increase in $\Delta V_{10\ mA\ cm^{-2}}$ was observed for fresh MEAs with HMT-PMBI-containing IrO_x anodes relative to the Nafion-only IrO_x-based MEAs (Table S2), with the increased overvoltages associated with slower TP-WS kinetics at the anode (Table S3), as well as a larger film resistance in the case of the IrO_x-30 MEA. This increase in series resistance is associated with the increased ionic resistance of HMT-PMBI (10 mS cm^{-1}) compared to Nafion (70 mS cm^{-1}) in the anode.[43]

A slight tailing in the Nyquist plot at low frequencies was observed, characteristic of a mass-transport limited process, potentially associated with OER operation under TP-WS conditions.[56] Calculations based on the limiting current density in steady-state polarization data suggest that this mass-transport limitation corresponds to a 10 mV overvoltage at 10 mA cm^{-2} (see SI for calculation). Degradation or neutralization of the HMT-PMBI film during electrolysis would also result in an increase in the series resistance. Degradation of HMT-PMBI would decrease the number sites available for OH^- transport, as well as potentially introduce H^+ transport pathways, with this increase in the series resistance being irreversible.[62] Neutralization of HMT-PMBI would decrease the mobile ion content in the catalyst film, where the initial conductivity of the MEA may be reobtained after soaking in electrolyte solution. Both pathways would result in an increase in the operating voltage at 10 mA cm^{-2} and could be observed utilizing *in situ* EIS analysis, with no change in the operating voltage upon rehydration. Rehydration of the IrO_x-10 MEAs resulting in the initial operating voltage (Figure S7). Further, no shift in the series resistance of IrO_x-10 samples was observed before and after constant-current electrolysis at 10 mA cm^{-2} over 16 h, indicating that minimal degradation or neutralization of HMT-PMBI occurred during operation of TP-WS in that time period.

iR-corrected TP-WS polarization data for IrO_x-based BPM MEAs are shown in Figure 7b, where the IrO_x-based BPMs overlap regardless of the HMT-PMBI content in the anode film. Both BPM MEAs, however, show increased ΔV_{act} at all currents measured relative to Pt|IrO_x-Nafion only MEAs (180 mV and 160 mV larger at 10 mA cm^{-2}, Table S2). Tafel plots for the IrO_x-based BPM MEAs are shown in Figure 7d, where both MEAs exhibit a linear region in the current density range of (1-10 mA cm^{-2}), corresponding to a Tafel slope of 226±11 and 220±10 mV dec^{-1} (n(1-α) = 0.27), much larger than characteristic Tafel slopes (120 mV dec^{-1} or less), that may in part be the result of convolution of OER kinetics with WD, as well as ionic transport losses in the MEA.[59]

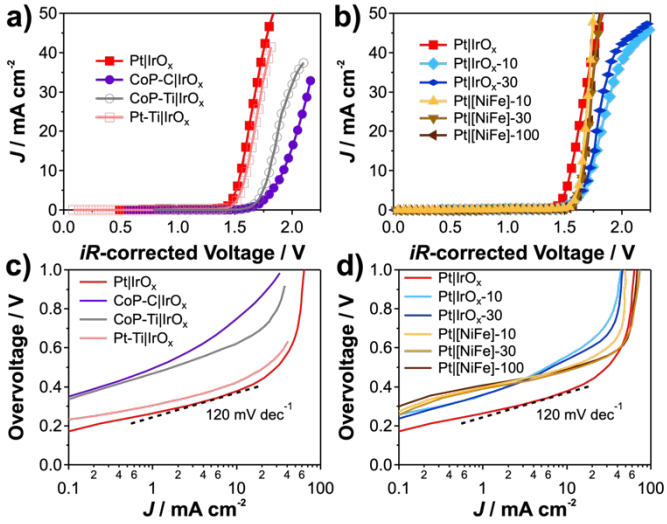

Figure 7. *iR*-corrected steady-state polarization data and Tafel plots for TP-WS under humid-N_2(g) flow at room temperature in a two-electrode configuration of a,c) Nafion MEAs using Pt/C on C-paper (3 mg cm^{-2}, red solid squares), Pt/C on Ti-paper (3 mg cm^{-2}, pink open squares), CoP on C-paper (2 mg cm^{-2}, purple solid circles), or CoP on Ti-paper (2.5 mg cm^{-2}, grey open circles) as the cathode with IrO_x on C-paper (3 mg cm^{-2}) as the anode; b,d) MEAs using IrO_x with a Nafion binder (red squares), IrO_x with 10 wt% HMT-PMBI (light blue diamonds), IrO_x with 30 wt% HMT-PMBI (dark blue diamonds), [NiFe]-LDH with 10 wt% HMT-PMBI (yellow triangles), [NiFe]-LDH with 30 wt% HMT-PMBI (gold triangles), or [NiFe]-LDH with 100 wt% HMT-PMBI (brown triangles) on C-paper as the anode, with Pt/C on C-paper (3 mg cm^{-2}) as the cathode. IrO_x loading of 3 mg cm^{-2}, [NiFe]-LDH loading of 0.6 mg cm^{-2}. Dashed line represents a Tafel slope of 120 mV dec^{-1} corresponding to an nα, or n(1-α), of 0.5.

3. [NiFe]-LDH Bipolar MEAs

The TP-WS characteristics of MEAs developed with [NiFe]-LDH anodes were strongly affected by the amount of HMT-PMBI in the catalyst films (Figure 6). During steady-state polarization, [NiFe]-LDH MEAs exhibited $V_{10\ mA\ cm^{-2}}$ values comparable to HMT-PMBI-based IrO_x MEAs, suggesting that the anode film is sufficiently alkaline to afford [NiFe]-LDH-based OER operation, but $\Delta V_{10\ mA\ cm^{-2}}$ was still 100 mV larger than for the Nafion-based Pt/C|IrO_x MEA (Table 1). The steady-state polarization data was independent of the HMT-PMBI content in the [NiFe]-LDH film. Under constant-current electrolysis at 10 mA cm^{-2}, the operating voltage increased substantially for both 10 and 30 wt% HMT-PMBI MEAs ([NiFe]-10, [NiFe]-30; Figure 5b, Table S3), becoming >2.4 V after 16 h. The initial operating voltage could not be reobtained after following the rehydration procedure, indicating anode catalyst film degradation during TP-WS (Figure S8). For the 100 wt% MEA ([NiFe]-100; Figure 5), $V_{10\ mA\ cm^{-2}}$ increased by only 150 mV over 16 h, indicating that sufficient HMT-PMBI was present to stabilize the [NiFe]-LDH over this time period (Table S3, Figure S7), but with the initial operating voltage not reobtained after the rehydration procedure. Consistently, further addition of HMT-PMBI did not have an additional stabilizing effect, nor did further rehydration attempts.

The initial EIS data of BPM [NiFe]-LDH MEAs at the operating voltage $V_{10\ mA\ cm^{-2}}$ required to drive TP-WS in a two-electrode configuration under humid-N_2(g) flow at room temperature are shown in Figure 5c, where similar to the IrO_x-based systems, two depressed semicircles are observed corresponding to the cathode and anode kinetics. The [NiFe]-LDH exhibited a smaller contribution to the EIS spectra than BPM-based IrO_x MEAs (Table S4), indicating that [NiFe]-LDH is able to perform OER more efficiently than IrO_x under TP-WS BPM-conditions. The series resistance was found to be independent of the HMT-PMBI loading, and comparable to the IrO_x-based Nafion-only MEAs. No tailing associated with mass-transport was observed at low frequencies, nor could the contribution of WD to the EIS spectra be determined here.

Analysis of EIS data under humid-N_2(g) flow at room temperature before and after constant-current electrolysis (10 mA cm^{-2}) under the same conditions (Figure 5c) indicated that the increase in $V_{10\ mA\ cm^{-2}}$ for [NiFe]-LDH with 100 wt% HMT-PMBI after constant-current electrolysis was associated with a decrease in the kinetics of the OER (200 mV increase in $\Delta V_{10\ mA\ cm^{-2}}$; Table S2, S3), because the cathode (Pt/C), Nafion membrane and HMT-PMBI were found to be stable under the same conditions. For [NiFe]-LDH with 30 wt% HMT-PMBI, however, the increase in the polarization resistance only accounted for 300 mV of the 600 mV increase in $V_{10\ mA\ cm^{-2}}$ after constant-current electrolysis (10 mA cm^{-2}; Table S2). Minimal to no change in the series resistance was observed in EIS studies for MEAs using [NiFe]-LDH anodes before or after electrolysis studies, indicating that the film degradation is the result of [NiFe]-LDH particle or [NiFe]-LDH|HMT-PMBI interface degradation rather than HMT-PMBI degradation during TP-WS operation, consistent with the IrO_x-based bipolar MEA results.

iR-corrected steady-state polarization data for [NiFe]-LDH MEAs is shown in Figure 7b. At low current densities, the [NiFe]-LDH MEAs exhibit a 100-120 mV larger ΔV_{act} relative to Pt|IrO_x-Nafion MEAs at 10 mA cm^{-2} (Table S2), but at higher current densities (>40 mA cm^{-2}), the [NiFe]-LDH begins to operate at smaller ΔV_{act} relative to the Pt|IrO_x-Nafion MEA. Analysis of the Tafel plot (Figure 7d) shows that the [NiFe]-LDH MEAs, regardless of HMT-PMBI content, exhibit a linear region from 1 to 30 mA cm^{-2}, with Tafel slopes ranging from 97±10 to 108±14 mV dec^{-1} ($n(1-\alpha) = 0.59$; Table 1). This Tafel slope suggests that the rate-limiting step is either the first or second electron transfer in the four-electron transfer pathway for water oxidation, consist with the observation that [NiFe]-LDH can undergo water oxidation more efficiently under alkaline conditions relative to IrO_x.[29] The value of the Tafel slope reported here could also be increased due to convolution with WD kinetics or ionic transport losses in the MEA.[60]

Nafion is acidic and in excess relative to the amount of HMT-PMBI used, so the additional protons might diffuse to, and neutralize the [NiFe]-LDH layer in the MEA over time and lead to catalyst activity loss.[29,63] An increase in the neutral region in the HMT-PMBI film near the Nafion interface can also occur provided WD is not occurring fast enough to maintain the applied current density, also resulting in catalyst activity loss. While this would have a minimal effect on the longevity of IrO_x films, it could have a substantial influence on the longevity of [NiFe]-LDH films. To prevent exposure of [NiFe]-LDH to the IL and Nafion, prior to MEA formation, a layer of HMT-PMBI was spin-cast on top of the [NiFe]-LDH film on the C-paper to test whether coating the [NiFe]-LDH in HMT-PMBI would protect against any acidic attack by Nafion or any film neutralization by interfacial layer growth. Figure S5 shows that adding HMT-PMBI to either the front or back sides of [NiFe]-LDH films did not have a beneficial effect on either the operating voltage or stability of Pt|[NiFe]-LDH MEAs during TP-WS in a two-electrode configuration under humid-N_2(g) flow at room temperature. Rather, the additional HMT-PMBI layer at the Nafion interface made the MEA more susceptible to dehydration effects during constant-current electrolysis.

Aliquots of 0.5 M KOH(aq) added to the [NiFe]-LDH side (no vapor flow on the OER side) of the MEA during constant-current electrolysis (10 mA cm^{-2}) in a two-electrode configuration caused a reduction in $V_{10\ mA\ cm^{-2}}$ from ~ 1.75 V to 1.65 V, with the durations at the lower voltage scaling with the amount of KOH introduced in each aliquot, suggesting catalyst film stabilization in the presence of excess base rather than excess water (Figure 8a). Anodes were then fed either humid-N_2(g) or with humid-N_2(g) and NH_3 (from N_2(g) bubbled through 1 M NH_4OH(aq) prior to entry into the anode side) at room temperature, but suffered from severe mass-transport limitations at 10 mA cm^{-2} (Figure 8b,c), with the MEA voltage increasing rapidly during constant-current electrolysis. Further addition of NaOH or KOH to the anode film in molar equivalents to the amount consumed under electrolysis prior to cell assembly did not result in an improvement in performance.

Discussion

Use of CoP in Nafion MEAs for TP-WS

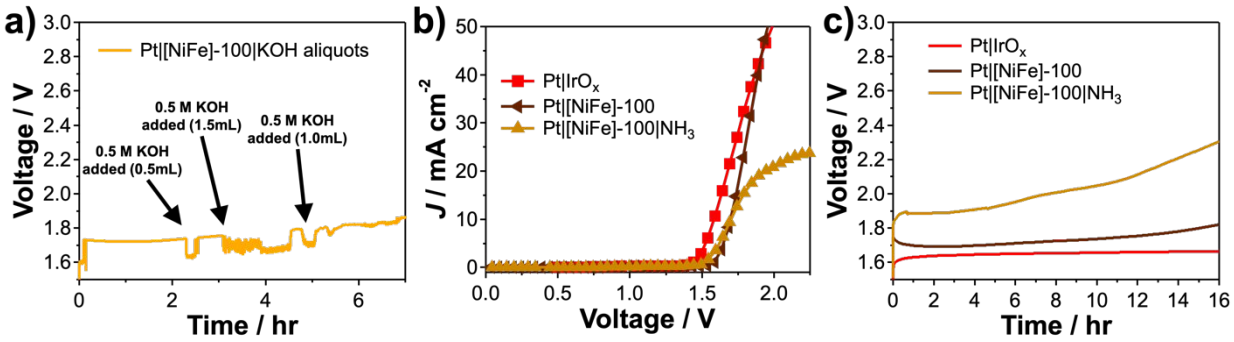

Figure 8. a) Constant-current electrolysis (10 mA cm^{-2}) data for room temperature TP-WS using a MEA coupling a Pt/C C-paper cathode to a [NiFe]-LDH anode with 100 wt% HMT-PMBI relative to [NiFe]-LDH. Aliquots of aqueous 0.5 M KOH were added to the anode side of the MEA at the times indicated, cathode side was under humid-N_2(g) flow. b) Steady-state polarization data and c) constant-current (10 mA cm^{-2}) electrolysis data for room temperature TP-WS using MEAs coupling Pt/C on C-paper (3 mg cm^{-2}) to [NiFe]-LDH (0.6 mg cm^{-2}) with 100 wt% HMT-PMBI (brown triangles) under humid-N_2(g) flow or under humid-N_2(g)-NH_3-flow (gold triangles). Nafion-based Pt/C|IrO_x MEA (red squares) under humid-N_2(g) flow shown for comparison.

Transition metal phosphide compounds have been the subject of interest for water-splitting applications due to their earth abundance and HER activity comparable to Pt.[64] Studies involving CoP-based systems for HER operation have typically used CoP synthesized directly on the surface of the electrode material (C-paper, Ti-paper, Si-surface) *via* either a flow reactor or using photoelectrochemical methods.[4,7,26] These processes are beneficial for small-scale devices and improve the electrical contact between the electrode and catalyst, but incorporation of CoP into commercial devices will require the development of scalable methods as well as methods to use low-cost substrates. Accordingly, we synthesized an activated form of nanoparticulate CoP as a powder, allowing the CoP film to be developed using standard catalyst-ink preparations, which can produce a porous structure necessary for efficient TP-WS by generating a large number of TPBs in the cathode film. The necessity of an additional Nafion overcoat to retain the CoP nanoparticles in all CoP-based MEAs investigated in this work, however, embedded the CoP nanoparticles in a Nafion matrix, reducing the porosity of the catalyst film and thereby reducing the number of TPBs available for HER operation (Figure 2b). A lack of porosity decreases the number of TPBs in the cathode film, decreasing the number of active CoP nanoparticle sites in the film at an applied voltage. While this reduction in TPBs did not alter the HER characteristics of CoP-Ti and CoP-C samples in acidic electrolyte studies, HER operation under TP-WS conditions was affected by the reduced number of active catalyst sites for HER operation in the film relative to Pt/C-based MEAs. A decrease in the number of active sites increases ΔV_{act} associated with TP-WS due to a lower effective J_0 of the film and can also increase $\Delta V_{polarization}$ due to slower kinetics.

The incorporation of CoP into catalyst ink preparations altered the observed HER kinetics both in acidic electrolyte and TP-WS studies, as evidenced by the potential/voltage-dependent Tafel slopes observed in this work. A potential/voltage dependent Tafel slope can be obtained if the film has poor electric/ionic conductivity due to the voltage gradient across the film and the corresponding gradient in catalyst utilization through the cathode film. As the voltage increases, more CoP within the film is utilized for HER operation, decreasing the observed Tafel slope until all of the CoP in the film is performing HER or until mass/ionic transfer effects are observed. The addition of C-black to CoP-C catalyst films decreased $\Delta V_{10\ mA\ cm^{-2}}$ by 50 mV (Figure S4) due to the increase in the electrical conductivity of the catalyst film and increase in the number of TPBs in the film. Formation of a CoP-electrical conductor composite powder, such as integration of CoP particles with carbon nanotubes, would not only increase the film conductivity and result in more CoP available for HER operation under TP-WS conditions, but also increase particle adhesion within the cathode film, properties vital for stable and efficient operation of TP-WS.[65,66]

The mass loadings used herein for both the CoP and the Pt/C catalysts were comparable in the cathode layers to perform TP-WS using MEAs in a two-electrode configuration. Given the reported surface areas for the CoP nanoparticles (59 m^2/g) and Pt/C (60 m^2/g) and the comparable mass loadings, the slower kinetics observed is also the result of lower turnover rates for CoP relative to Pt in both configurations. These kinetic losses dominated $\Delta V_{polarization}$ in EIS studies of CoP-based MEAs performing TP-WS under humid-N_2(g) flow at room temperature (Figure 5a).[26] Based on EIS studies in a two-electrode configuration under room temperature humid-N_2(g) flow, an additional overvoltage due to an increased series resistance was observed for MEAs using a CoP/Ti-paper cathode relative to MEAs with a CoP/C-paper cathode, and can be attributed to an increase in the contact resistance between the graphite channel plates and the Ti-paper. A larger Tafel slope was observed for CoP MEAs (152±16 mV dec^{-1}) relative to Pt/C MEAs (121±16 mV dec^{-1}) under TP-WS operation, consistent with the results in acidic electrolyte studies, and would result in a slight increase ΔV_{act} for TP-WS in a two-electrode configuration. An increase in the ΔV_{act} for TP-WS is also expected based on J_0 for CoP to perform HER in acidic electrolyte (0.1 mA cm^{-2}) relative to Pt (0.9 mA cm^{-2}) in a three-electrode configuration.[26]

A larger drift (90-190 mV) in $V_{10\ mA\ cm^{-2}}$ was observed in CoP-based MEAs under TP-WS operation relative to Pt-based MEAs (50 mV drift) after 16 h of electrolysis. For CoP-C MEAs, the initial operating voltage could be reobtained after rehydration,

but EIS studies after rehydration of the MEA indicate slower kinetics for HER operation, corresponding to the 30 mV increase in $\Delta V_{polarization}$ observed. This increase could be associated with particle aggregation/loss and a reduction in the number of TPBs over the course of electrolysis. For CoP-Ti MEAs, the initial operating voltage could not be reobtained after rehydration, suggesting that particle aggregation/loss is the predominant source for the drift in the operating voltage. CoP nanoparticles could also be slowly oxidized by water during HER operation under TP-WS conditions, increasing the overvoltage and potentially altering the mechanism by which the catalyst performs HER.[27,28]

Bipolar MEAs for TP-WS

Given the potential to simultaneously maintain locally acidic and locally alkaline conditions, respectively, in two distinct physical regions of a BPM, we investigated the stability of a BPM towards TP-WS by using a recently developed, solution-processable AEM, HMT-PMBI,[43] in the anode of the MEA. The conductivity and stability of the bipolar MEA then becomes dependent on the HMT-PMBI content in the anode film. As shown in Figures 6 and 7, an increase in the operating voltage to perform TP-WS was observed for bipolar IrO_x-based MEAs relative to Nafion-based IrO_x MEAs, independent of HMT-PMBI content, associated with slower TP-WS kinetics due to a potential reduction in catalyst utilization in the anode films relative to a Nafion-based MEA, increased ionic transport losses in the anode film due to the use of HMT-PMBI (10 mS cm^{-1}) instead of Nafion (70 mS cm^{-1}) as the ionomer,[43] and due to WD in the BPM IL. The overvoltage associated with WD in unoptimized Nafion|HMT-PMBI membranes to pass 10 mA cm^{-2} has been reported to be 200 mV when in contact with liquid electrolyte, similar to the 100-250 mV increase in the overvoltage observed in this work for bipolar MEAs relative to monopolar MEAs operating TP-WS at 10 mA cm^{-2} (Table 1).[45] This suggests that the increased ΔV_{act} observed for bipolar MEAs is due to WD, where WD can influence the Tafel analysis of bipolar MEAs under TP-WS operation. An increase in the Tafel slope from 55 mV dec^{-1} for IrO_x operation in alkaline electrolyte in a three-electrode configuration to 220 mV dec^{-1} for TP-WS operation in a two-electrode configuration is not expected based on changes in mechanism or ionic transport losses alone, and may be the result of the convolution of WD and OER kinetics.[60] The total cell voltage for bipolar MEAs studied in this work (1.7-1.8 V, Table 1) to pass 10 mA cm^{-2} is comparable to voltages obtained for a vapor-fed MEA utilizing an AEM,[22] as well as a solution-fed CoP|[NiFe]-LDH BPM under a pH gradient,[8] where a similar drift in the cell voltage (50 mV over 16 h) was observed under constant-current electrolysis at 10 mA cm^{-2}, associated with gradual loss of the pH gradient.

The drift in the operating voltage (30-60 mV) of the bipolar MEAs during constant-current electrolysis was found to be the result of MEA dehydration, similar to the behaviour of Nafion-only MEAs studied in this work, rather than membrane degradation, as no irreversible increase in the series resistance or operating voltage after TP-WS electrolysis was observed. Dehydration of a bipolar MEA can result in: a decrease in the ionic conductivity (series resistance) and the mobility of species in the MEA (polarization resistance), which can impact the pH gradient between the anode and cathode films, increasing the overvoltage, as well as increase the IL thickness (i.e., increase the size of the neutral region) due to impeded WD, assuming a well-defined BPM junction. An increase in the IL thickness will increase the neutral, non-ionically conducting region deplete of mobile ions in the anode, increasing $\Delta V_{polarization}$ during TP-WS operation due to the reduced amount of OER catalyst still ionically connected in the anode. Bipolar MEAs exhibited a similar drift in the operating voltage over the same time period and at the same applied current density as the Nafion-only MEAs of this work, suggesting a similar mechanism associated with the voltage drift observed. Dehydration of monopolar MEAs results in a decrease in the ion mobility, resulting in a change in the pH at the cathode and anode. Similarly, a decrease in the ionic mobility of bipolar MEAs occurs due to dehydration, which will decrease the pH gradient between the anode and cathode films. A 50 mV drift would correspond to a decrease in the pH gradient of 1 pH unit, with the initial pH conditions (0-1 at the cathode, 13-14 at the anode) being reinstated upon rehydration.

The pH gradient and IL growth can also be affected by the presence of OER catalyst at the BPM interface, where the catalyst particles can act as 'pinholes' or potentially facilitate WD. As shown in Figure 3, for IrO_x-based bipolar MEAs, the predominant surface species of the anode film is HMT-PMBI, where IrO_x is embedded within the polymer matrix, indicating that a BPM interface with minimal 'pinholes' is generated in bipolar IrO_x MEAs. Studies of Nafion-HMT-PMBI BPM membranes in solution also demonstrated stable pH gradients over the same time period at the same current density, indicating that the permselectivity of both ionomers is preserved both when in contact with electrolyte solution or during TP-WS.[45]

Use of [NiFe]-LDH in bipolar MEAs for TP-WS

The [NiFe]-LDH used in this work was produced using pulse-laser ablation techniques, which can generate readily scalable and highly tunable, high-surface-area powders (chemical formulat $[Ni_{0.78}Fe_{0.22}(OH)_2](NO_3^-)_{0.22}\bullet nH_2O$ here), that show high activity towards OER operation under alkaline conditions.[44] Although the primary method for IrO_x incorporation into MEAs uses Nafion as the ionomer in the catalyst layer, using the same approach for [NiFe]-LDH would result in degradation due to exposure of the catalyst to a locally acidic environment. This instability might be mitigated through the use of an alkaline ionomer on the anode side of the MEA. We therefore formed a bipolar MEA to evaluate the performance of [NiFe]-LDH as an anode catalyst layer for room temperature humid-N_2(g) fed TP-WS. The catalytic performance of the [NiFe]-LDH thus depended on the availability of base to maintain a high effective local pH in the HMT-PMBI layer during TP-WS under humid-N_2(g) flow at room temperature, as well as the capabilities of the BPM to perform WD under the operating conditions.

The initial operating voltage for all [NiFe]-LDH BPM MEAs was found to be comparable to IrO_x-based bipolar MEAs (Figure 6), with smaller Tafel slopes, consistent with studies in alkaline electrolyte in a three-electrode configuration (Figure 3), indicating that HMT-PMBI initially provides a sufficiently alkaline environment for OER operation by [NiFe]-LDH under TP-WS conditions. The operating voltage required to drive TP-WS using bipolar MEAs with [NiFe]-LDH anodes incorporating 10 or 30 wt% HMT-PMBI relative to [NiFe]-LDH, however, increased substantially over time. No loss in [NiFe]-LDH particles was observable after electrolysis, and bipolar [NiFe]-LDH MEAs incorporating 100 wt% HMT-PMBI or IrO_x MEAs with HMT-PMBI were stable under the same conditions. EIS studies indicated that only 300 mV of the 600 mV increase in $V_{10\ mA\ cm^{-2}}$ observed for MEAs containing [NiFe]-LDH with 30 wt% HMT-PMBI during a constant-current electrolysis (10 mA cm^{-2}) was due to an increase in $\Delta V_{polarization}$ due to impeded OER operation at the anode (Figure 5). No change in the series resistance was observed, indicating that HMT-PMBI is intact, and that Ni/Fe dissolution and transport into the Nafion is not the predominant degradation mechanism.[63] We thus attribute the additional increase in $V_{10\ mA\ cm^{-2}}$ observed for [NiFe]-LDH bipolar MEAs to changes in the environment (local pH, carbonate concentration) local to the [NiFe]-LDH in the film, catalyst degradation (forming $NiOOH/NiFeO_x$),[44] or gradual particle aggregation and reduced resulting TPB in the anode, similar to recent reports.[67]

As the HMT-PMBI content increases in the [NiFe]-LDH film, the surface of the film that interacts with the Nafion membrane has less [NiFe]-LDH exposed on the surface (Figure 3), resulting in a more defined BPM interface. This would result in (i) reduced degradation of [NiFe]-LDH due to less direct exposure to Nafion, (ii) an increase in the interfacial area capable of performing WD, increasing the OH^- content of the anode film and decreasing the neutral IL region in the anode, (iii) better maintenance of the pH gradient during TP-WS operation due to a smaller presence of [NiFe]-LDH 'pinholes' at the BPM interface. The stability of the [NiFe]-LDH MEA during TP-WS was found to increase as the HMT-PMBI loading was increased up to 100 wt% relative to the catalyst. [NiFe]-LDH films with 100 wt% HMT-PMBI exhibit a similar morphology to HMT-PMBI containing IrO_x anodes, where the predominant surface species is HMT-PMBI, while the exposure of [NiFe]-LDH increases as the HMT-PMBI content decreases. The presence of [NiFe]-LDH at the interface will decrease the area associated with WD at the BPM interface, resulting in a larger neutral region within the anode film, and decrease the pH of the anode film via proton diffusion from Nafion through the [NiFe]-LDH pinholes. This decrease in the pH of the anode will decrease the activity of [NiFe]-LDH towards OER under TP-WS conditions, increasing the operating voltage due to slower kinetics and less catalyst utilization, and degrade [NiFe]-LDH catalyst particles at these more acidic pH values until device failure.[29] IrO_x is stable in both alkaline and acidic environments, and would not be irreversibly degraded under the same conditions. Attempts at providing an external source of base did not stabilize the [NiFe]-LDH anode layer in the MEA during TP-WS (Figure 8). Addition of an HMT-PMBI layer between the anode film and the Nafion membrane may prevent catalyst degradation but suffers from severe dehydration effects during TP-WS operation (Figure S5).

Influence of carbonate on bipolar MEA-based TP-WS

Prior studies of HMT-PMBI have shown that the OH^- form of HMT-PMBI rapidly generates carbonate ions under ambient conditions.[43] The OER activity and stability of [NiFe]-LDH exposed to 1 M aqueous KOH under ambient conditions was enhanced by incorporation of carbonate generated from CO_2 in solution, and is also expected to be generated during the MEA preparation steps in this work.[68] This was also observed during TP-WS in this work, where MEAs developed using the Br^- form of HMT-PMBI instead of the OH^- form, allowing the OH^- form to develop during TP-WS, exhibited both larger operating voltages and lower stability towards TP-WS under constant-current electrolysis (Figure S6).

Under TP-WS operation, carbonate removal from the catalyst film can occur due to the generation of OH^- in the IL and the necessity for electroneutrality in the ionomer-based catalyst film. The slow removal of carbonate anions from the [NiFe]-LDH catalyst film could contribute to the gradual decrease in performance observed herein, and potentially lead to catalyst particle degradation through removal of carbonate from the [NiFe]-LDH structure.[29,68] AEM-based and BPM-based fuel cell studies have observed carbonate removal from the MEA at the anode *via* a 'self-purging' mechanism ($CO_3^{2-} + H_2 \rightarrow CO_2 + H_2O + 2e^-$), with minimal contribution to the current being passed (<0.005%) during electrolysis tests.[69–72]

A 'self-purging' mechanism may operate during MEA-based TP-WS, where instead of H_2, carbonate removal is coupled with OH^- consumption ($2OH^- + CO_3^{2-} \rightarrow O_2 + CO_2 + H_2O + 4e^-$). Given the dimensions of our cell, the timescale and current density of electrolysis tests, and the rates of carbonate removal from previous studies at similar current densities, consumption of the carbonate in the HMT-PMBI film would only account for <1.7% of the current passed during electrolysis tests (assuming a constant rate of consumption over 16 h, see SI for calculation). Preliminary *in situ* mass spectra of the anode exhaust of a bipolar MEA during TP-WS operation indicate the presence of both CO_2 and CO alongside O_2 production and is the subject of further investigation. No carbon-based products were observed in the anode exhaust of a monopolar MEA under the same conditions, suggesting that the carbon-based products are not due to the oxidation of C-paper at the anode. [NiFe]-LDH was also deposited onto Ti-paper, stainless steel, and gold-coated substrates to eliminate C from the anode, but either produced high-resistance contacts due to oxidation of the electrode material or did not catalyze the OER when tested in contact with a liquid alkaline electrolyte.

Optimization strategies

All MEAs investigated in this work exhibited a dependence on the hydration level of the membrane over the course of electrolysis, corresponding to a 50 mV increase over 16 h at 10 mA cm^{-2}. The operating voltages, as well as the lifetime of the MEAs prior to rehydration, are optimal for coupling to a

photovoltaic system, such as a perovskite solar cell, under 1 Sun AM 1.5G illumination, where 16 h corresponds to operation under these conditions through the course of a day.[8] The operating voltages for monopolar and bipolar MEAs to effect TP-WS at room temperature under humid-N_2(g) flow (1.6-1.7 V), is comparable to other monopolar MEA systems under the same conditions.[13,22] Operation of the MEAs with intermittent use to afford MEA rehydration (e.g. 16 h ON, 0.5-8 h OFF) will offer insight as to the longevity of devices over more realistic timespans when coupled to a photovoltaic system (>100 h), as well as afford operation protocols for long-term (>1000 h) continuous operation on a grid system. Alternatively, the MEAs could be operated at elevated pressures and temperatures, where the membrane and catalyst films may exhibit better hydration and higher conductivities, increasing the voltage efficiency for TP-WS and afford larger current densities.[63]

The electrolysis of water vapor utilizing a photoelectrochemical (PEC) system may ease design constraints, where the requirement of liquid electrolyte, and issues associated with product bubble formation are minimized. Here, stable operation of TP-WS under a pH gradient was observed, with operating voltages comparable to BPM-based electrolyzer systems in contact with liquid electrolyte.[8] In a fully-integrated PEC system, the catalyst loading and distribution on the photoelectrodes will need to optimized to minimize light absorption and scattering. Instead of liquid electrolyte, an ionomer will need to coat the photoelectrodes to afford TP-WS under TP-WS conditions. The membrane thickness and porosity will also need to be optimized to ensure minimal light absorption/scattering, product crossover, and maintain the pH gradient. Under the flow rate conditions used (0.2 LPM on each electrode side), the O_2 concentration in the exhaust produced at a current density of 10 mA cm^{-2} was determined to be 600 ppm (production rate of $7.8x10^{-8}$ mol s^{-1}), and given the O_2 permeabilities of HMT-PMBI ($0.3x10^{-12}$ mol cm^{-1} s^{-1})[73] and Nafion N117 ($2x10^{-12}$ mol cm^{-1} s^{-1}),[5] some product crossover is expected, but is in competition with convection and diffusion of O_2 from the anode film into the gas stream, driven by the humid-N_2(g) flow.

Ensuring the integrity of the BPM interface will also be vital when utilizing MEA-based TP-WS, as was seen prominently with the [NiFe]-LDH MEAs in this work. Design of anode materials that exhibit a layer of an AEM that affords intimate contact with the CEM, with a porous catalyst layer facing the anode gas diffusion electrode, would provide a well-defined WD interface without pinholes while ensuring sufficient TPBs to afford efficient TP-WS in the anode film. Such 'protective' layers were attempted in this work by spin-casting HMT-PMBI on top of [NiFe]-LDH anodes prior to MEA formation but suffered from hydration issues (Figure S5) and potential reductions in the number of TPBs in the anode film. Further optimization of the morphology and thickness of the alkaline anode film may improve the performance, as well as introducing a WD catalyst, such as graphene oxide, to the BPM interface to improve WD kinetics under TP-WS operation.[74]

Conclusions

The earth-abundant catalysts CoP and [NiFe]-LDH can be integrated into MEAs that effect room temperature TP-WS at a current density of 10 mA cm^{-2} under humid-N_2(g) flow. MEAs constructed from Nafion with CoP nanoparticles on the cathode and IrO_x on the anode were stable for > 16 h of continuous TP-WS at 10 mA cm^{-2} under humid-N_2(g) flow, but required substantially larger operating voltages, $V_{10\ mA\ cm^{-2}}$, (1.95±0.05 V) when compared to MEAs with Pt/C on the cathode (1.59±0.01 V), due to fewer available triple-phase boundaries and slower kinetics under TP-WS operation, in comparison to the small difference (20 mV) in overpotentials, $\eta_{-10\ mA\ cm^{-2}}$, of these cathode materials in contact with 0.50 M H_2SO_4(aq). [NiFe]-LDH was mixed with a solution-processable AEM, HMT-PMBI, and incorporated into MEAs with Pt/C-Nafion cathodes, creating a bipolar MEA. When a sufficient amount of HMT-PMBI was used, the bipolar MEA with [NiFe]-LDH was stable for 16 h of continuous TP-WS at a current density of 10 mA cm^{-2} under humid-N_2(g) flow. MEAs using [NiFe]-LDH integrated with HMT-PMBI as the anode exhibited similar $V_{10\ mA\ cm^{-2}}$ values (1.70±0.01V) to MEAs using IrO_x integrated with HMT-PMBI as the anode (1.74±0.02V), with bipolar MEAs exhibiting an additional overvoltage (100-200 mV) relative to a Nafion-only MEA due to the formation of a BPM. The [NiFe]-LDH films were less stable than IrO_x films, with the stability of the [NiFe]-LDH films dependent on the HMT-PMBI content of the MEA, associated with the anode film morphology and ability of the resulting BPM to maintain a pH gradient. Bipolar MEAs with IrO_x were stable under the same operating conditions, where no HMT-PMBI degradation was observed, and a 1 pH unit shift in the pH gradient observed. All MEAs exhibited a drift in the overvoltage during constant-current electrolysis due to dehydration.

Future work will focus on developing and utilizing transition metal phosphides integrated with nanoparticulate electrical conductors to increase the electrical conductivity and promote catalyst adhesion within catalyst-ink-based films, increasing the longevity and efficiency of HER operation under TP-WS conditions. The development of a well-defined BPM interface that also maintains a porous catalyst film morphology with minimal impact on the resistance of the MEA will also be investigated, criteria necessary for stable BPM-based TP-WS operation using pH sensitive catalysts.

Conflicts of interest

There are no conflicts to declare.

Acknowledgements

Support for this work was provided by the United States National Science Foundation (NSF) under the CCI Solar Fuels Program, Grant No. CHE-1305124. We are grateful to Kimberly Papadantonakis for helpful comments and technical editing of the manuscript.

References

1 N. S. Lewis and D. G. Nocera, *Proc. Natl. Acad. Sci.*, 2006, **103**, 15729–15735.
2 N. S. Lewis, *Nat. Nanotechnol.*, 2016, **11**, 1010–1019.
3 M. G. Walter, E. L. Warren, J. R. McKone, S. W. Boettcher, Q. Mi, E. A. Santori and N. S. Lewis, *Chem. Rev.*, 2010, **110**, 6446–6473.
4 T. R. Hellstern, J. D. Benck, J. Kibsgaard, C. Hahn and T. F. Jaramillo, *Adv. Energy Mater.*, 2016, **6**, 1501758.
5 K. Sun, R. Liu, Y. Chen, E. Verlage, N. S. Lewis and C. Xiang, *Adv. Energy Mater.*, 2016, **6**, 1600379.
6 E. Verlage, S. Hu, R. Liu, R. J. R. Jones, K. Sun, C. Xiang, N. S. Lewis and H. A. Atwater, *Energy Environ. Sci.*, 2015, **8**, 3166–3172.
7 C. W. Roske, E. J. Popczun, B. Seger, C. G. Read, T. Pedersen, O. Hansen, P. C. K. Vesborg, B. S. Brunschwig, R. E. Schaak, I. Chorkendorff, H. B. Gray and N. S. Lewis, *J. Phys. Chem. Lett.*, 2015, **6**, 1679–1683.
8 J. Luo, D. A. Vermaas, D. Bi, A. Hagfeldt, W. A. Smith and M. Grätzel, *Adv. Energy Mater.*, 2016, **6**, 1600100.
9 K. A. Walczak, G. Segev, D. M. Larson, J. W. Beeman, F. A. Houle and I. D. Sharp, *Adv. Energy Mater.*, 2017, **7**, 1602791.
10 S. Ardo, S. H. Park, E. L. Warren and N. S. Lewis, *Energy Environ. Sci.*, 2015, **8**, 1484–1492.
11 T. S. Sinclair, H. B. Gray and A. M. Müller, *Eur. J. Inorg. Chem.*, 2018, 1060–1067.
12 M. B. McDonald, J. P. Bruce, K. McEleney and M. S. Freund, *ChemSusChem*, 2015, **8**, 2645–2654.
13 J. M. Spurgeon and N. S. Lewis, *Energy Environ. Sci.*, 2011, **4**, 2993–2998.
14 R. O'Hayre, D. M. Barnett and F. B. Prinz, *J. Electrochem. Soc.*, 2005, **152**, A439–A444.
15 S. Z. Oener, S. Ardo and S. W. Boettcher, *ACS Energy Lett.*, 2017, **2**, 2625–2634.
16 S. A. Grigoriev, V. I. Porembsky and V. N. Fateev, *Int. J. Hydrogen Energy*, 2006, **31**, 171–175.
17 C. Xiang, K. M. Papadantonakis and N. S. Lewis, *Mater. Horizons*, 2016, **3**, 169–173.
18 S. L. McFarlane, B. A. Day, K. McEleney, M. S. Freund and N. S. Lewis, *Energy Environ. Sci.*, 2011, **4**, 1700–1703.
19 M. A. Modestino, M. Dumortier, S. M. Hosseini Hashemi, S. Haussener, C. Moser and D. Psaltis, *Lab Chip*, 2015, **15**, 2287–2296.
20 S. Kumari, R. Turner White, B. Kumar and J. M. Spurgeon, *Energy Environ. Sci.*, 2016, **9**, 1725–1733.
21 J. Rongé, S. Deng, S. Pulinthanathu Sree, T. Bosserez, S. W. Verbruggen, N. Kumar Singh, J. Dendooven, M. B. J. Roeffaers, F. Taulelle, M. De Volder, C. Detavernier and J. A. Martens, *RSC Adv.*, 2014, **4**, 29286–29290.
22 G. Heremans, C. Trompoukis, N. Daems, T. Bosserez, I. F. J. Vankelecom, J. A. Martens and J. Rongé, *Sustain. Energy Fuels*, 2017, **1**, 2061–2065.
23 J. Rongé, D. Nijs, S. Kerkhofs, K. Masschaele and J. A. Martens, *Phys. Chem. Chem. Phys.*, 2013, **15**, 9315–9325.
24 B. M. Hunter, H. B. Gray and A. M. Müller, *Chem. Rev.*, 2016, **116**, 14120–14136.
25 J. R. McKone, S. C. Marinescu, B. S. Brunschwig, J. R. Winkler and H. B. Gray, *Chem. Sci.*, 2014, **5**, 865–878.
26 E. J. Popczun, C. G. Read, C. W. Roske, N. S. Lewis and R. E. Schaak, *Angew. Chemie - Int. Ed.*, 2014, **53**, 5427–5430.
27 Y. Zhang, L. Gao, E. J. M. Hensen and J. P. Hofmann, *ACS Energy Lett.*, 2018, **3**, 1360–1365.
28 J. Tian, Q. Liu, A. M. Asiri and X. Sun, *J. Am. Chem. Soc.*, 2014, **136**, 7587–7590.
29 S. Anantharaj, K. Karthick and S. Kundu, *Mater. Today Energy*, 2017, **6**, 1–26.
30 I. A. Moreno-Hernandez, C. A. Macfarland, C. G. Read, K. M. Papadantonakis, B. S. Brunschwig and N. S. Lewis, *Energy Environ. Sci.*, 2017, **10**, 2103–2108.
31 M. J. Kirshenbaum, M. H. Richter and M. Dasog, *ChemCatChem*, 2019, 1–6.
32 M. Ünlü, J. Zhou and P. A. Kohl, *J. Phys. Chem. C*, 2009, **113**, 11416–11423.
33 M. B. McDonald, S. Ardo, N. S. Lewis and M. S. Freund, *ChemSusChem*, 2014, **7**, 3021–3027.
34 N. M. Vargas-Barbosa, G. M. Geise, M. A. Hickner and T. E. Mallouk, *ChemSusChem*, 2014, **7**, 3017–3020.
35 D. A. Vermaas, M. Sassenburg and W. A. Smith, *J. Mater. Chem. A*, 2015, **3**, 19556–19562.
36 D. M. Weekes, D. A. Salvatore, A. Reyes, A. Huang and C. P. Berlinguette, *Acc. Chem. Res.*, 2018, **51**, 910–918.
37 D. A. Vermaas and W. A. Smith, *ACS Energy Lett.*, 2016, **1**, 1143–1148.
38 T. P. Pandey, A. M. Maes, H. N. Sarode, B. D. Peters, S. Lavina, K. Vezzu, Y. Yang, S. D. Poynton, J. R. Varcoe, S. Seifert, M. W. Liberatore, V. Di Noto and A. M. Herring, *Phys. Chem. Chem. Phys.*, 2015, **17**, 4367–4378.
39 Q. Duan, S. Ge and C.-Y. Wang, *J. Power Sources*, 2013, **243**, 773–778.
40 D. A. Salvatore, D. M. Weekes, J. He, K. E. Dettelbach, Y. C. Li, T. E. Mallouk and C. P. Berlinguette, *ACS Energy Lett.*, 2018, **3**, 149–154.
41 J. R. Varcoe, P. Atanassov, D. R. Dekel, A. M. Herring, M. A. Hickner, P. A. Kohl, A. R. Kucernak, W. E. Mustain, K. Nijmeijer, K. Scott, T. Xu and L. Zhuang, *Energy Environ. Sci.*, 2014, **7**, 3135–3191.
42 K. Zhang, M. B. McDonald, I. E. A. Genina and P. T. Hammond, *Chem. Mater.*, 2018, **30**, 6420–6430.
43 A. G. Wright, J. Fan, B. Britton, T. Weissbach, H.-F. Lee, E. A. Kitching, T. J. Peckham and S. Holdcroft, *Energy Environ. Sci.*, 2016, **9**, 2130–2142.
44 B. M. Hunter, J. D. Blakemore, M. Deimund, H. B. Gray, J. R. Winkler and A. M. Müller, *J. Am. Chem. Soc.*, 2014, **136**, 13118–13121.
45 S. Chabi, A. G. Wright, S. Holdcroft and M. S. Freund, *ACS Appl. Mater. Interfaces*, 2017, **9**, 26749–26755.
46 R. A. Rozendal, H. V. M. Hamelers, R. J. Molenkamp and C. J. N. Buisman, *Water Res.*, 2007, **41**, 1984–1994.
47 T. Shinagawa, A. T. Garcia-Esparza and K. Takanabe, *Sci. Rep.*, 2015, **5**, 1–21.
48 J. O. Bockris, *J. Chem. Phys.*, 1956, **24**, 817–827.
49 A. I. Krasil'shchikov, *Zh. Fiz. Khim*, 1963, **37**, 273.

50 C. Hu, L. Zhang and J. Gong, *Energy Environ. Sci.*, , DOI:10.1039/c9ee01202h.
51 L. Trotochaud, S. L. Young, J. K. Ranney and S. W. Boettcher, *J. Am. Chem. Soc.*, 2014, **136**, 6744–6753.
52 M. E. G. Lyons and S. Floquet, *Phys. Chem. Chem. Phys.*, 2011, **13**, 5314–5335.
53 M. Gong, Y. Li, H. Wang, Y. Liang, J. Z. Wu, J. Zhou, J. Wang, T. Regier, F. Wei and H. Dai, *J. Am. Chem. Soc.*, 2013, **135**, 8452–8455.
54 E. Fabbri, A. Habereder, K. Waltar, R. Kötz and T. J. Schmidt, *Catal. Sci. Technol.*, 2014, **4**, 3800–3821.
55 S. Siracusano, N. Van Dijk, E. Payne-Johnson, V. Baglio and A. S. Aricò, *Appl. Catal. B Environ.*, 2015, **164**, 488–495.
56 C. Rozain and P. Millet, *Electrochim. Acta*, 2014, **131**, 160–167.
57 I. Dedigama, P. Angeli, K. Ayers, J. B. Robinson, P. R. Shearing, D. Tsaoulidis and D. J. L. Brett, *Int. J. Hydrogen Energy*, 2014, **39**, 4468–4482.
58 J. Durst, C. Simon, F. Hasché and H. A. Gasteiger, *J. Electrochem. Soc.*, 2015, **162**, F190–F203.
59 L. G. Austin, *Trans. Faraday Soc.*, 1964, **60**, 1319–1324.
60 M. L. Perry, J. Newman and E. J. Cairns, *J. Electrochem. Soc.*, 2006, **145**, 5–15.
61 Z. Yan, L. Zhu, Y. C. Li, R. J. Wycisk, P. N. Pintauro, M. A. Hickner and T. E. Mallouk, *Energy Environ. Sci.*, 2018, **11**, 2235–2245.
62 R. He, Q. Li, G. Xiao and N. J. Bjerrum, *J. Memb. Sci.*, 2003, **226**, 169–184.
63 M. Carmo, D. L. Fritz, J. Mergel and D. Stolten, *Int. J. Hydrogen Energy*, 2013, **38**, 4901–4934.
64 J. F. Callejas, C. G. Read, C. W. Roske, N. S. Lewis and R. E. Schaak, *Chem. Mater.*, 2016, **28**, 6017–6044.
65 Q. Liu, J. Tian, W. Cui, P. Jiang, N. Cheng, A. M. Asiri and X. Sun, *Angew. Chemie*, 2014, **126**, 6828–6832.
66 Y. Pan, Y. Lin, Y. Chen, Y. Liu and C. Liu, *J. Mater. Chem. A*, 2016, **4**, 4745–4754.
67 D. Xu, M. B. Stevens, M. R. Cosby, S. Z. Oener, A. M. Smith, L. J. Enman, K. E. Ayers, C. B. Capuano, J. N. Renner, N. Danilovic, Y. Li, H. Wang, Q. Zhang and S. W. Boettcher, *ACS Catal.*, 2019, **9**, 7–15.
68 B. M. Hunter, W. Hieringer, J. R. Winkler, H. B. Gray and A. M. Müller, *Energy Environ. Sci.*, 2016, **9**, 1734–1743.
69 S. Watanabe, K. Fukuta and H. Yanagi, *ECS Trans.*, 2010, **33**, 1837–1845.
70 Z. Siroma, S. Watanabe, K. Yasuda, K. Fukuta and H. Yanagi, *J. Electrochem. Soc.*, 2011, **158**, B682–B689.
71 K. Fukuta, H. Inoue, S. Watanabe and H. Yanagi, *ECS Trans.*, 2009, **19**, 23–27.
72 A. Pătru, T. Binninger, B. Pribyl and T. J. Schmidt, *J. Electrochem. Soc.*, 2019, **166**, F34–F43.
73 D. Novitski, A. Kosakian, T. Weissbach, M. Secanell and S. Holdcroft, *J. Am. Chem. Soc.*, 2016, **138**, 15465–15472.
74 M. B. McDonald and M. S. Freund, *ACS Appl. Mater. Interfaces*, 2014, **6**, 13790–13797.